Solveig Aasheim Johansen

Optimization of Energy Saving Devices

Master's thesis in Marine Technology
Supervisor: Kourosh Koushan
June 2020

Master's thesis

NTNU

Norwegian University of
Science and Technology

Solveig Aasheim Johansen

Optimization of Energy Saving Devices

Master's thesis in Marine Technology
Supervisor: Kourosh Koushan
June 2020

Norwegian University of Science and Technology
Faculty of Engineering
Department of Marine Technology

NTNU
Norwegian University of
Science and Technology

MASTER THESIS IN MARINE TECHNOLOGY

SPRING 2020

FOR

Solveig Aasheim Johansen

OPTIMIZATION OF ENERGY SAVING DEVICES

Energy saving devices are applied to ships to improve the energy efficiency of the vessels. These devices can be fitted to new builds as well as retrofitted to existing vessels. Depending on the type and design of the device as well as details of the vessel and the propeller, savings could be up to 10%. If the device is not properly optimised for the vessel and her operating condition, it might even result in worsening the efficiency. Therefore, customisation and optimisation of the device is important for its performance. One type of these devices is Pre-Swirl Stator, consisting of usually 3-5 fins placed in front of the propeller. This device can improve the inflow to the propeller. At the same time the device also changes the flow and pressure distribution at the aft part of the vessel. There are several parameters which can be optimised. It is also important to study the scale effects on performance of these devices, because the performance is often measured in model scale. In addition, PSS can be combined with PBCF (Propeller boss cap fins) to improve the efficiency further.

The candidate shall use a chemical tanker as test case. PSS shall be optimised for this vessel using computational fluid dynamic (CFD) methods. Parameters to be optimised include number of fins, angular position of fins, pitch of fins, profile shape and axial position of PSS. Then the candidate shall study application of PBCF to the same vessel. Optimisation will be performed also for PBCF using CFD. The CFD analysis can be performed using SIEMENS commercial code STAR CCM+. However, the candidate might also use other software including propeller design and analysis software. Effect of PSS and PBCF on cavitation performance of the propeller and on the devices shall be discussed. Scale effect on PSS and PBCF shall be elaborated and discussed.

In the thesis the candidate shall present his personal contribution to the resolution of problem within the scope of the thesis work.

Theories and conclusions shall be based on mathematical derivations and/or logic reasoning identifying the various steps in the deduction.

The thesis work shall be based on the current state of knowledge in the field of study. The current state of knowledge shall be established through a thorough literature study, the results of this study shall be written into the thesis. The candidate should utilize the existing possibilities for obtaining relevant literature.

The thesis should be organized in a rational manner to give a clear exposition of results, assessments, and conclusions. The text should be brief and to the point, with a clear language. Telegraphic language should be avoided.

The thesis shall contain the following elements: A text defining the scope, preface, list of contents, summary, main body of thesis, conclusions with recommendations for further work, list of symbols and acronyms, reference and (optional) appendices. All figures, tables and equations shall be numerated.

The supervisor may require that the candidate, in an early stage of the work, present a written plan for the completion of the work. The plan should include a budget for the use of computer and laboratory resources that will be charged to the department. Overruns shall be reported to the supervisor.

The original contribution of the candidate and material taken from other sources shall be clearly defined. Work from other sources shall be properly referenced using an acknowledged referencing system.

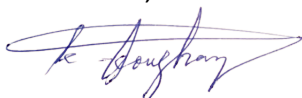The thesis shall be submitted electronically (pdf) in NTNU IT system:

- Signed by the candidate
- The text defining the scope (signed by the supervisor) included
- Computer code, input files, videos and other electronic appendages can be uploaded as a zip file and shall be provided in addition on an electronic storage.
- Any electronic appendages shall be listed in the main thesis.

Supervisor : Professor Kourosh Koushan

Start : 15.01.2020

Deadline : 10 June 2020 at 14:00.

Trondheim, 15.01.2020

Kourosh Koushan
Supervisor

Preface

This Master's thesis has been carried out at the department of Marine Technology at the Norwegian University of Science and Technology, NTNU, during the spring of 2020. This thesis is the final work towards my M.Sc. degree, where I specialize within hydrodynamics. During the fall of 2019, I did a preparatory project for the master's thesis with a literature study on pre-swirl stators and use of CFD in design optimization. This provided the basis for much of the theory presented in this thesis, and was of great help to get the master's thesis started.

Regardless of the theory I had studied before I started this master's thesis, I quickly understood the importance of experience in numerical computations and how important it is to have a deep understanding of CFD to obtain adequate results. Throughout the project there has been many trial and errors, and I have met different challenges during the study. This spring semester has been especially affected by the global pandemic, COVID-19, with closed campus and working from home. It has been of much help to study reports from earlier projects similar to mine and using tutorials from Star-CCM+.

I would like to thank my supervisor Kourosh Koushan for giving me a challenging, yet interesting project for my master's thesis. I would also thank Lucia Sileo and Mariusz Przybylski for helping me get started in Star-CCM+ and sharing tips and tricks along the way.

Solveig A. Johansen

Solveig Aasheim Johansen

Trondheim, 10.06.2020

Abstract

Due to environmental awareness and an increase in fuel prices, there has been an increasing demand for new technology to improve ship's energy efficiency to reduce fuel consumption. One of the simplest and most effective methods to improve fuel efficiency is to improve propulsion performance. This could be done in several ways, but one measure is to implement energy saving devices that are designed to optimize the propeller efficiency. One type of energy saving devices that improve propeller efficiency is pre-swirl stators. The PSS usually consists of 3-5 fins, designed to manipulate the inflow to the propeller to make it more homogeneous, and thus increase propeller efficiency.

The objective of this thesis is to optimize a pre-swirl stator used on a chemical tanker. By improving the propeller efficiency, the energy consumption of the ship will decrease. Through an optimization study on design parameters such as fin radius, angular position of fins, and the pitch angle of the fins, the best PSS design configuration will be found. The hydrodynamic performance for the different configurations is found through numerical calculations in Star-CCM+. By systematically varying the design parameters one by one and investigating how the hydrodynamic performance is influenced, the optimal design is found for the pre-swirl stator.

All simulations conducted for this study is performed using Star-CCM+. By implementation of different physical models, the chemical tanker is simulated with and without the presence of free surface. The free surface simulation is performed as a part of the validation study of the numerical set-up. The optimization process is performed without free-surface to save computational time. The numerical set-up is validated through a comparison of the resistance coefficient and the nominal wake of another numerical study conducted on the same ship. Results from these comparisons showed good agreements between the two studies.

16 different pre-swirl design configurations were investigated in the optimization process. By systematic variation of the design parameters, the various configurations were investigated through numerical computations. Through a study of the increased propeller efficiency, increased ship resistance and the wake field, the optimal design configuration is found. From the results it is found that all PSS configurations give some increase in propeller efficiency. The optimal solution provides a increased propeller efficiency of 8.51% relative to the propeller without PSS, and 3.85% more than the initial PSS configuration. This configuration increases the average relative resistance with 4.72% compared to the ship without PSS. Since the study was carried out with a fixed rotational velocity of the propeller, the resistance increased when the thrust increased.

From the simulation of the optimal configuration, the influence of the PSS is visualized. From these figures, it is visible how the PSS alters the flow around the aft ship. The streamlines show that the PSS cancels out the vortex from flow separation in front of the propeller, and the pressure coefficient is plotted to evaluate the cavitation domains.

Samandrag

Som følgje av auka fokus på klima og høgare drivstoffprisar, har det dei siste tiåra vore ein veksande etterspurad etter ny teknologi for å betre energieffektiviteten til skip. Ein av dei enklaste og mest effektive metodane for å få ned drivstofforbuket for eit skip, er ved å optimalisere propulsjonssystemet. Det finns ei rekkje tiltak som senkar drivstofforbruket, og eit av tiltaka ein kan nytte er å implementere energisparande einingar som er designa for å optimalisere propulsjonseffektiviteten. Ein type energisparingseining er pre-swirl stators, frå no av referert til som PSS. Ein PSS består av tre til fem finnar som er plassert framfor propellen, og er designa til å manipulere strøyminga inn i propellen. Ved å få ei meir homogen strøyming inn i propellen vil verknadsgraden til propellen gå opp, og ein vil minske energiforbruket til skipet.

Målet med denne masteroppgåva er å optimalisere ein PSS som blir brukt på eit kjemikalietankskip. Gjennom eit optimaliseringsstudie vil ulike designparametrar som finne-radius, vinkelposisjon og pitch-vinkel bli variert slik at det optimale designet kan bli identifisert. Dei hydrodynamiske kreftene som verkar på systemet vil bli funne gjennom numeriske berekningar i Star-CCM+. Ved å implementere ulike fysiske modellar i den virtuelle slepetanken, vil tankskipet bli simulert både med og utan fri overflate. Simuleringa som er utført med fri overflate er gjort som ein del av valideringsprosessen for det numeriske oppsettet. Optimaliseringsprosessen for finnane er utført utan fri overflate for å spare køyretid i kalkuleringane.

16 ulike designkonfigurasjonar er undersøkt for å finne det optimale PSS-designet. Frå resultata i simuleringane ser ein at alle designkonfigurasjonane gir auka propellverknadsgrad samanlikna med propellen utan PSS. Det optimale designet gir ein auka propellverknadsgrad på 8.5%, som er 3.85% høgare enn for det originale designet av PSS. Den relative motstanden er også auka med 4.72%, som følge av auka thrust og konstant skipshastigheit og propulsjonshastigheit.

Frå simuleringane av det optimale PSS-designet kan ein sjå korleis strøyminga blir påverka av finnane. Frå resultata kan ein sjå at virvelen som oppstår på grunn av avløysning framfor propellen blir løyst opp av finnane. Det er også tydeleg at krafta til virvelen bak propellnavet minkar. Trykkoeffisienten på propellblada endrar seg også, så kavitasjonsdomena på propellblada blir undersøkt.

Table of Contents

List of Tables

List of Figures

Nomenclature

Δy [m]   Half cell height for first cell

δ [m]   Boundary layer thickness

η_P [-]   Propeller efficiency

μ [$Pa \cdot s$]   Dynamic viscosity

ν [m^2/s]   Kinematic viscosity

ρ [kg/m^3]   Density of substance

σ [-]   Cavitation number

τ_w [Pa]   Wall shear stress

C_F [-]   Friction coefficient

C_P [-]   Pressure coefficient

CFD Computational Fluid Dynamics

D [m]   Propeller diameter

DNS Direct Numerical Simulation

ESD Energy Saving Device

J [-]   Advance number

L_{PP} [m]   Length between perpendiculars

LES Large Eddy Simulation

n [rps]   Rate of revolutions

NS Navier-Stoke

p_∞ [Pa]   Free stream pressure

p_V [Pa]   Vapor pressure

$PBCF$ Propeller Boss Cap fins

PID Propulsion Improving Devices

PSS Pre-Swirl Stator

Q $[N \cdot m]$ Torque

Qn [-]   Propulsion performance index

R_{TS} [N]   Ship resistance

$RANS$ Reynolds-Averaged Navier-Stoke

Re [-]   Reynolds number

T $[N]$ Thrust

V_{∞} [m/s]   Free stream velocity

V_a [m/s]   Relative velocity

v_a [m/s]   Axial velocity component

v_r [m/s]   Radial velocity component

V_S [m/s]   Ship velocity

v_t [m/s]   Tangential velocity component

$y+$ [-]   Non-dimensional wall distance

Chapter 1

Introduction

Due to environmental awareness and an increase in fuel prices, there has been an increasing demand for new technology to improve ships' energy efficiency over the last decades. With increased attention to the environmental footprint from burning fossil fuels, there has been a growing interest in reducing the fuel consumption of ships. Contributing initiatives to reduce the shipping industry's emissions are stricter regulations and financial intensives for reducing emissions. Large amounts of money are granted for research on measures to reduce fuel consumption; thus, many innovative devices that increase the energy efficiency of ships have been introduced. Some fuel-reducing measures are hull form optimization, hydrodynamic energy-saving devices that aim to improve the ship's propulsive efficiency, structural optimization, and reducing the weight of the vessel. One of the simplest and most effective methods to improve fuel efficiency is to improve propulsion performance (Park et al., 2015). Improvement of the machinery technology and optimizing the operational measures for ships in operation is essential to reduce the fuel consumption (ABS, 2013).

Several types of energy saving devices are designed to optimize the propeller efficiency for new builds as well as retrofit ships in operation. Examples of such devices can be pre-swirl devices, post-swirl devices, wake equalizing, and flow separation alleviating devices. Energy-savings can be as high as 10% depending on the type and design of the energy-saving device, details of the vessel, and the propeller (ABS, 2013). For poorly designed devices the efficiency might be decreased, so it is critical to fit the ESD to all individual ships.

One type of energy saving device is pre-swirl stators (PSS), usually consisting of 3-5 fins located in front of the propeller. The pre-swirl stator alters the inflow to the propeller by modifying the axial and tangential velocity components of the inflow to the propeller. The most significant amount of energy saving comes from recovering parts of the kinetic energy losses associated with tangential velocities (Koushan et al., 2020). Reduced kinetic losses and improved inflow to the propeller give improved propeller efficiency and thus reduce the ship's fuel consumption.

1.1 Objective

This master thesis will focus on optimizing a pre-swirl stator used on a chemical tanker. There are several parameters to be optimized; the radius of the fins, angular position of fins, and the pitch angle of the fins. By utilizing Computational Fluid Dynamics (CFD) tools, different configurations of the parameters are investigated to find the optimal design for the PSS. The objective is to maximize the increase in propeller efficiency, so that the fuel consumption of the chemical tanker is reduced.

The design optimization is performed for full-scale conditions for design speed and draught. The flow into the propeller depends on the hull shape, propeller, rudder and energy saving devices. Since so many factors influence the flow, the numerical calculations must be considered as one system. To accurately capture the interaction between the hull, PSS, rudder, and propeller, the propeller rotation is simulated as rigid body motion as this provides the most accurate results. The optimization of PSS will be executed by systematically comparing the results from the CFD-analyses, and in the optimization process, each parameter's best configuration will be found one by one and then used for the remainder of the simulations. The effect of the PSS on the cavitation performance of the propeller will be investigated and discussed. The CFD analyses are performed using the commercial code Star-CCM+.

Originally, as stated in the contract, it was intended to investigate the potential of implementing propeller boss cap fins in combination with the pre-swirl stator used in this thesis. The PBCF is energy saving device that is compatible with PSS, and could be designed to make use of the remaining energy in the hub vortex. The unpredictable situation this spring with the pandemic, and challenges related to that situation, the simulation process got delayed, and there was no time for such study. A short section with theory behind the working principles of the PBCF will be presented to understand how the PBCF could influence the flow.

1.2   Use of CFD in ESD optimization

Computational fluid dynamics, CFD, has become a widely used tool to predict the hydrodynamic performance of ships. CFD gives the opportunity to investigate both the macroscopic forces in a system and the details in the ship's flow field. Therefore, CFD can be used to predict the full scale wakefield and is particularly helpful when studying the ESD's influence on the flow around the hull. CFD tools can also assist in the optimization process of a design since they allow multiple iterations. Hull form, hydrodynamic energy-saving devices, propeller, and rudder can be optimized by analyzing how different variations of the parameters will influence the efficiency of the ship.

CFD is also valuable when studying the complex flow around the hull. Historically, ships have been studied in model scale using towing tanks, but this makes it difficult and expensive to investigate the details of the wake. Due to scale-effects on the wakefield, the extrapolated model-scale results tend to vary from the sea-trials. When studying devices that work in the ship's boundary layer, such as pre-swirl stators, the scale effects play a significant role. It has been noted that the energy gain of the PSS predicted from model-scale differs from the results from sea-trials. Koushan et al. found that the energy saving for the PSS in model scale differs quite a lot from the full-scale CFD and sea-trial results with energy savings of 2.5% and 4.0% respectively (Koushan et al., 2020). The analyses in this thesis will therefore be based on running CFD in full-scale.

1.3   Research on PSS

There are many available research reports on pre-swirl stators and the challenges of designing a PSS. Studies that evaluates different trials will be discussed below.

Nowruzi and Najafi did a combined experimental and numerical study on the effect the PSS has on the propulsion performance using different types of pre-swirl ducts (Nowruzi and Najafi, 2019). In this research, three different types of pre-swirl ducts were tested; the Mewis duct, Becker twisted fins and an unconventional half-circular duct as shown in Figure 1.1a, 1.1b and 1.1c. To investigate the propulsion performance, thrust and torque coefficients, efficiency components of the intended propulsion system, wake and pressure distributions were evaluated. They found that the PSS performance varies with the advance ratio. For lower advance ratios the Becker twister fins provided highest thrust and torque coefficients, while for higher advance ratios Mewis ducts provided the highest value of the coefficients. They also found that inflow to the pre-swirl ducts is highly dependent on the ship's hull form, and that it is difficult to establish a general guideline for design and position of pre-swirl ducts.

(a) Mewis duct   **(b)** Becker twisted fins   **(c)** Unconventional half circular duct
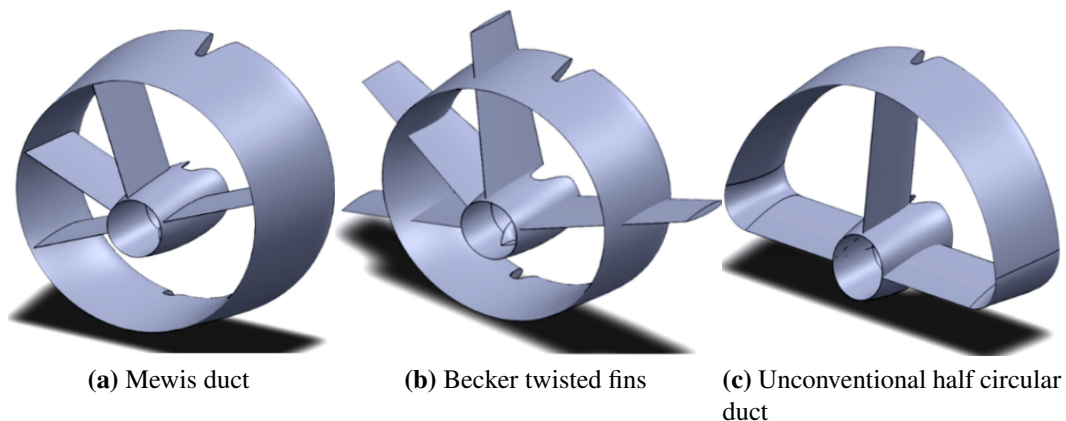
Figure 1.1: Three different configurations of pre-swirl ducts (Nowruzi and Najafi, 2019)

Koushan et al. performed a numerical and experimental investigation of different designs of pre-swirl stators on a chemical tanker (Koushan et al., 2020). Different designs were studied through systematically varying the design parameters such as fin geometry parameters and installation parameters. 70 alternative design solutions were analyzed to find the highest power-savings. The power-saving was found to be up to 4% for the best configuration. Figure 1.2a, 1.2b and 1.2c show three different variations of the PSS design from this study. It was found that studying the kinetic flow energy in the propeller slipstream is useful to understand the working principle of the PSS. Additionally, the axial wake fraction must be studied since swirl assessment alone is not sufficient for the ESD performance analysis. The report points to the importance of careful adaptation of ESD to see which PSS would give the largest power-saving. This study was performed both experimentally and numerically. For the numerical simulation, STAR-CCM+ was used, and the models used for the simulations are described thoroughly in the report.

| (a) Var-1 | (b) Var-3 | (c) Var-5 |
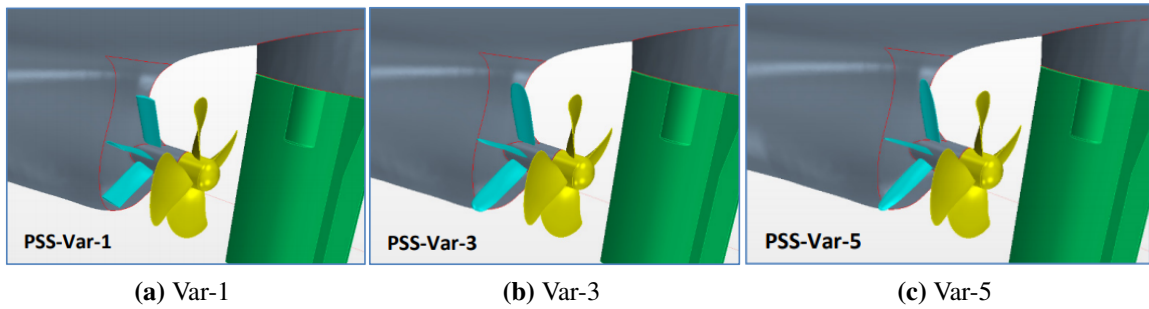
Figure 1.2: Three different configurations of pre-swirl stators (Koushan et al., 2020)

Kim et al. performed hydrodynamic optimization of a pre-swirl stator by CFD and model testing. This paper describe the process from the developments of the PSS in the early design stage, optimization process, model tests and at last a validation of the results through sea trial tests (Kim et al., 2013). This study uses a simple design of the PSS and optimizes the design by varying the fin parameters. The optimization study for this research uses a relatively straightforward approach. The design parameters are systematically varied one parameter at a time, and the optimal parameter is determined based on the propulsion performance index, Qn. The optimization process finds the optimal value for one parameter and keeps the value for the remainder of the simulations going further to the next parameter. This optimization model does not include the coupled effect between the different parameters, but it does save considerable amounts of computational time since each parameter requires a substantial CPU time.
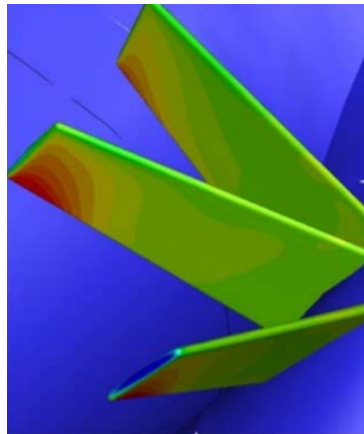
Figure 1.3: Stator fins (Kim et al., 2013)

Dang et al. used CFD calculations and model tests to get a better understanding of the working principle of different types of energy saving devices (Dang et al., 2012). Dang et al. studies the influence of the ESDs on thrust, resistance and shaft rotational speed, as well as the energy balance in front of and behind the propeller. The results from the CFD analyses are compared to the experimental results and was found to be quite consistent. From these results Dang et al. propose principles of a guideline for ESD designs for single screw merchant ships, where the most important point is that the ESDs should be optimized with regards to the kinetic energy in the downstream wake.

2

Theoretical foundation

This chapter presents the theoretical foundation used for the numerical optimization of the pre-swirl stators. The hydrodynamic performance of the propeller is studied through multiple numerical simulations. This chapter introduce the theoretical foundation needed for the optimization of the PSS, including both propeller theory and numerical theory. Some of these subjects was studied in the project thesis on energy saving devices, thus, parts of the theory presented here originates from that project (Johansen, 2019).

2.1 Propeller performance

2.1.1 Propeller performance characteristics

It is crucial to understand the characteristics of the propeller performance when optimizing the effect of energy saving devices as the characteristics are used to compare the various configurations. The performance characteristics of a propeller can be divided into open water properties, and behind-hull properties (Carlton, 2007). The performance of the propeller is defined by some general non-dimensional parameters that express the forces and moments generated by the propeller. The open water parameters of the propeller are obtained from open water tests in towing tanks or CFD analyses. The non-dimensional terms are as follows;

$$\text{Thrust coefficient: } K_T = \frac{T}{\rho n^2 D^4} \tag{2.1}$$

$$\text{Torque coefficient: } K_Q = \frac{Q}{\rho n^2 D^5} \tag{2.2}$$

$$\text{Advance number: } J = \frac{Va}{nD} \tag{2.3}$$

$$\text{Cavitation number: } \sigma = \frac{p_\infty - p_V}{\frac{1}{2}\rho V^2} \tag{2.4}$$

Equation 2.1 is related to the delivered thrust of the propeller, T. The number of revolutions, n, water density, ρ, and the propeller diameter, D, is known. Torque coefficient in Equation 2.2 use the same entities, and all of them are known except for the torque, Q, that must be found in the open water tests or simulation.

From Equation 2.3 it is seen that the advance number, J, depends on the speed of advance, V_a, rotational speed n, and diameter, D. V_a is the freestream velocity of the ship. The diameter

of a propeller is constant, but the rotational speed and speed of advance can be varied.

Cavitation number, σ, is a dimensionless number that are used to to investigate if the flow has the potential to cavitate. The cavitation number express the pressure difference between the local absolute pressure and the vapor pressure.

Other terms that are important to the propeller performance are delivered power and propeller efficiency. Delivered power is a function of the torque on the propeller as seen in Equation 2.5. The propeller efficiency is given as the relationship between the thrust force and delivered power and express the required amount of power needed to deliver a level of thrust. The propeller efficiency is given in Equation 2.6.

$$\text{Delivered power: } P_D = 2\pi n Q \tag{2.5}$$

$$\text{Propeller efficiency: } \eta_o = \frac{TV_a}{2\pi n Q} = \frac{J}{2\pi}\frac{K_T}{K_Q} \tag{2.6}$$

An open water diagram can be used to plot the propeller performance characteristics for different values of the advance number. A typical open water diagram for fixed pitch propellers working in a non-cavitating environment at a positive advance coefficient is shown in Figure 2.1. The figure shows multiple plots for the operating conditions at positive advance number, J, and rotational speed, n at different pitch ratios P/D (Carlton, 2007). One can also see how the change of the pitch ratio influences the characteristics. For a specific fixed-pitch propeller, there will only be one curve for each of the parameters, K_T, K_Q, and η.
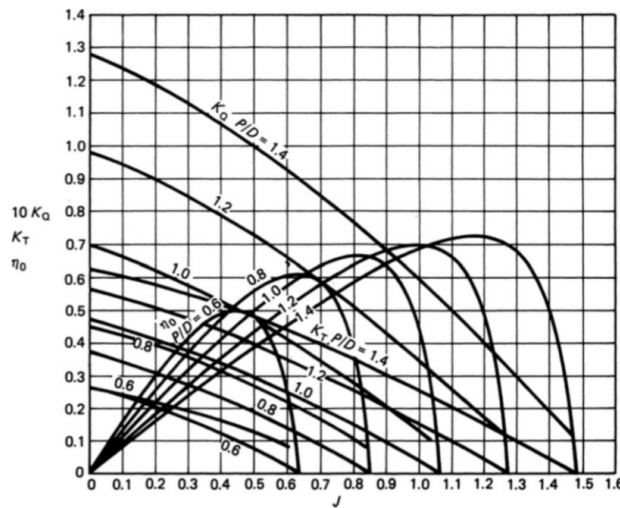
Figure 2.1: Open water diagram for the Wageningen B5-75 screw series (Carlton, 2007)

From Equation 2.3 one can see that the advance number varies with the advance velocity, V_a. That means that if the advance velocity decrease, so will the advance number, J. Figure 2.1 shows curves for the efficiency, η, as a function of the advance number. In cases of decreased rotational speed or increased velocity, the advance number increases, thus propeller efficiency is improved and thrust and torque coefficients decrease.

2.1.2   Wake field

When a body moves through water, the motion causes a wake field behind the body. This means that there are disturbances in the flow that leads to an uneven velocity distribution behind the body. The flow field varies with time and spatially and it is affected by the upstream geometry. The wake field at the propeller plane has three main contributions; the streamline flow around the body, the growth of the boundary layer over the body, and the influence of any wave-making components (Carlton, 2007).

The ships hull shape and appendages strongly influence the wake field. In general, single-screw ships have wake fields characterized by a strongly non-uniform distribution of velocities with a wake peak at the top position (Regener et al., 2018). That means that the blade sections of a propeller operating behind the ship experience substantial variations in the angle of attack. For propeller design, it is desired to have as homogeneous wake field as possible, so that the propeller blades operate at optimal angle at all positions as it rotate.

To understand the data from the wake field plots, the data can be defined using different methods. There are three main principal methods; the velocity ratio method, Taylor method, and Froude methods (Carlton, 2007), where the former one is the most commonly used. The velocity ratio method use iso-velocity contours expressed as a ratio of the ship speed V_S and the velocity of a point in the propeller disc. The velocity in the propeller disc is expressed in terms of the axial, tangential, and radial components, v_a, v_t and v_r, respectively.

$$\frac{v_a}{V_S}, \frac{v_t}{V_S} \text{ and } \frac{v_r}{V_S} \tag{2.7}$$

Figure 2.2 illustrates the axial and in-plane velocity ratio. The axial velocity ratio are presented using iso-lines, and the in-plane velocity ratio are presented using gradient vectors with a direction and a length.
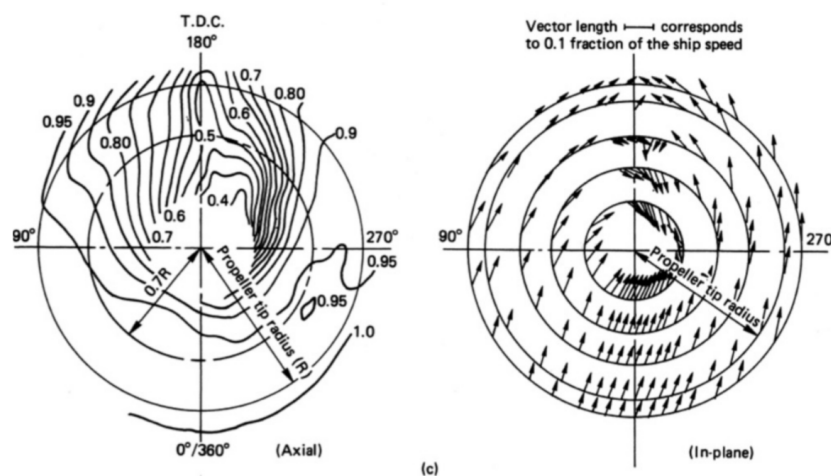
Figure 2.2: Axial velocity ratio and in-plane velocity ratio (Carlton, 2007)

2.1.3 Nominal and effective wake field

The nominal wake field is the wake field that would be measured at the propeller plane without the presence or influence of a propeller. The nominal wake field of a ship can be considered to be a compromise of the potential wake, the wave-induced wake, and the frictional wake (Carlton, 2007). The potential wake component is the wake that arise if the ship was in an inviscid fluid. The wave action component originates from the movement of water particles in the system of gravity waves at the ship by the water surface. The frictional wake field occur as the fluid of viscous nature flow past the hull surface. This component is derived from the growth of the boundary layer over the hull surface. Figure 2.3a show the transverse nominal wake field at the propeller plane. Here the flow is not influenced by a propeller or other appendages to disrupt the flow. Figure 2.3b show how the nominal flow changes when a pre-swirl stator is implemented. The flow is notably altered at the port side of the ship. The figures are from Dang et al.s study of the working principles of energy saving devices (Dang et al., 2012).

(a) Transverse nominal wake field on the propeller plane without ESDs

(b) Transverse nominal wake field on the propeller plane with ESDs
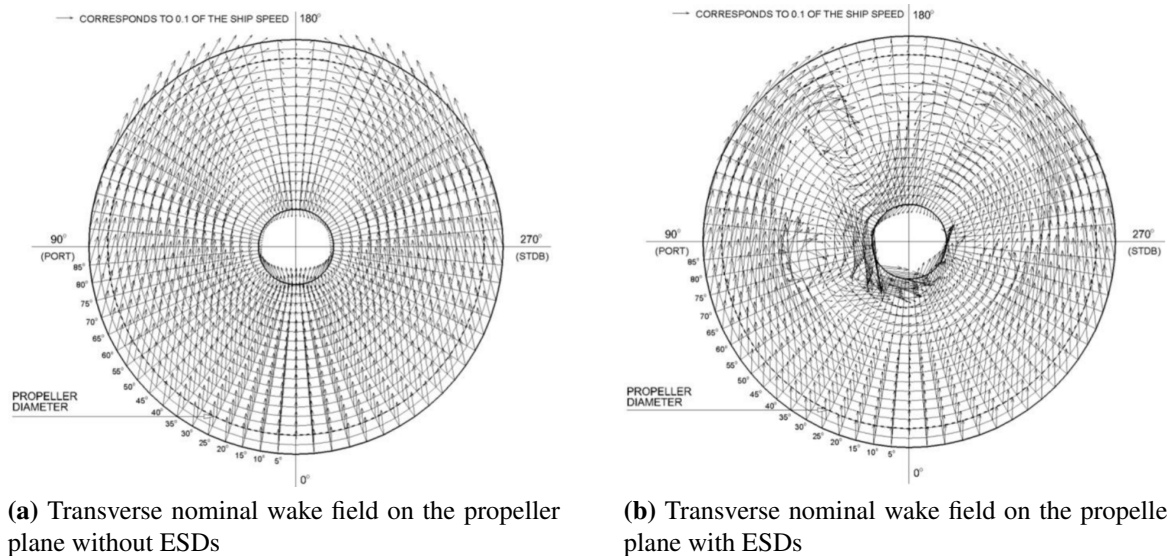
Figure 2.3: Transverse wake field (Dang et al., 2012)

When the propeller is operating behind the hull, the flow becomes more complex than for the nominal wake situation. Due to complicated interactions between the hull and the rotating propeller, the flow field in the effective wake is not simply the sum of the flow in the absence of the propeller, together with the propeller-induced velocities calculated based on the nominal wake (Carlton, 2007). The effective wake is a result of the contribution from three components; the flow from the naked hull, the propeller induced flow and the interaction of the two. The effective wake field is used as input for analyses in the design process and must be found through iterative processes.

2.1.4 Optimal wake field for propeller

Since propellers operate in a complex flow field influenced by the hull geometry, appendages, and an interaction component, all ships have individual wake fields. Because the velocity varies both in radial and tangential directions, the velocity field experienced by a blade section will

vary along a rotation (Savio, 2011). When the propeller operates in the stern, the velocity field will vary throughout a revolution due to disturbance in the flow field, making it complicated to design a propeller that works optimally throughout the entire revolution. It is desired to have as homogeneous wake flow distribution as possible at the propeller plane, so that the relative difference between the maximum and minimum velocity is small and there is not abrupt transition in the fluid.

It is desired to design a propeller that is operating optimally for all angles, but this is not possible when the relative velocities change over the revolution. Various energy-saving devices can be used to improve the transverse nominal wake, so that the propeller works at more optimal conditions over a larger part of the revolution. A transverse nominal wake field without ESDs, is shown in Figure 2.3a. For a propeller rotating clockwise, the propeller blades will experience higher relative velocities along the starboard side. In Figure 2.3b the transverse nominal field wake on the propeller disc with ESD is shown. When comparing these two nominal wakes, it is seen that the ESD changes the velocity profile so that the direction of the velocities on port side are changed, thus the relative velocity to the propeller is increased. This may result in higher provided thrust. Figure 2.4a show a typical nominal axial velocity distribution for a single screw ship. Figure 2.4b shows how the axial velocity varies along radial section r/R=0.68 over one revolution.

(a) Axial velocity   (b) Velocity profile along radial section r/R = 0.68
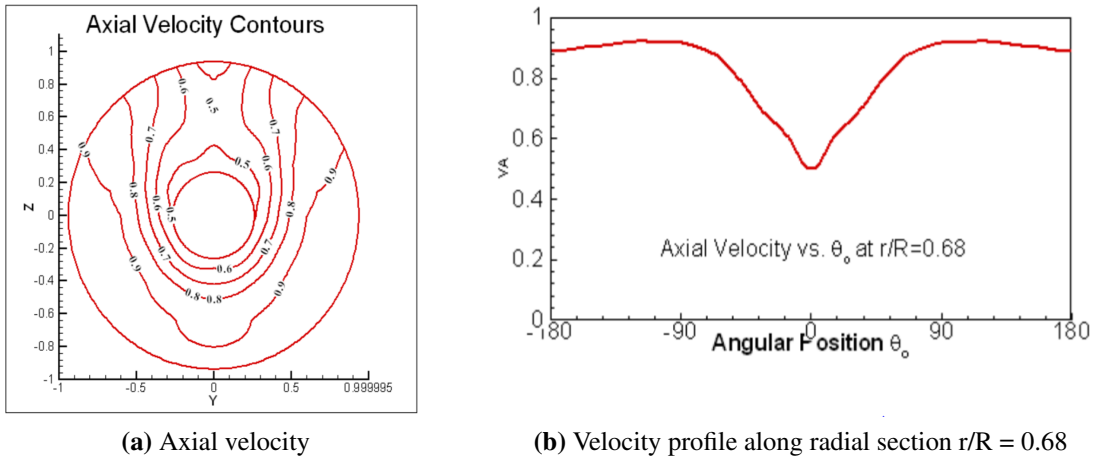
Figure 2.4: Typical nominal axial wake field for a single-screw container ship (Kerwin, 2001)

The wake field must be considered when investigating the risk of propeller cavitation. Large velocity disruptions should also be avoided to avoid large pressure jumps, that may lead to cavitation on the propeller. Caviation happens where the local variations in velocity are large. For instance, in regions of low axial velocity, the parts of the blade may experience reduced advance velocities and sheet cavitation can occur (Savio, 2011).

2.2 Computational fluid dynamics

2.2.1 Star-CCM+

STAR CCM+ is a commercial CFD-software developed by CD-adapco, designed to run large simulation efficiently. The software implements object-oriented programming allowing both beginners and experts to utilize the CFD software. The software covers the entire simulation process, including CAD modeling, CAD embedding, surface preparation tools, automatic meshing models, physics modeling, turbulence modeling, and post-processing of the results from the simulation (CD-Adapco, 2016).

Star-CCM+ provides a range of options that makes it possible to solve the Navier-Stokes equations. These include multiple Reynolds Averaging models (RANS), Large Eddy Simulation (LES), Detached Eddy Simulation (DES), and inviscid potential flow. More details of the models used in the simulations will be presented in the following sections of this chapter.

2.2.2 Governing equations

Computational Fluid Dynamics is based on three governing equations; Continuity equation, Navier-Stokes equation, and the Energy equation. To analyze the motion of the fluid particles in the domain, the equations of motion must be solved. For a viscous, laminar, incompressible, Newtonian fluid without free-surface effects the equations of motion are the continuity equation and the Navier-Stokes equation (Cengel and Cimbala, 2010). The general continuity equation is given as

$$\vec{\nabla} \cdot \vec{V} = \frac{\partial u}{\partial x} + \frac{\partial v}{\partial y} + \frac{\partial w}{\partial z} = 0 \tag{2.8}$$

And the Navier-Stokes equation is given by

$$(\vec{\nabla} \cdot \vec{V})\vec{V} = -\frac{1}{\rho}\vec{\nabla}P' + \nu\nabla^2\vec{V} \tag{2.9}$$

Equation 2.8 is a conservation equation and Equation 2.9 is a transport equation that represents the transport of momentum throughout the computational domain (Cengel and Cimbala, 2010). The fluid of interest is assumed to be incompressible, thus the continuity equation and the moment equation are uncoupled from the energy equation. That means that there are four coupled differential equations to solve for four unknowns; u,v,w and p.

2.2.3 RANS Solver

The Reynolds-averaged Navier–Stoke equations, or the RANS equations, are time-averaged equations of motion for fluid flow. The RANS-solver use an averaging technique, where the solver calculates a constant value of the velocity as well as a fluctuating value (Pettersen, 2019). A RANS-solver will be used in this master thesis, and the Navier-Stoke Equations will therefore be discussed in greater details. To solve the Navier-Stokes for one velocity component, Equation 2.10 is used, where i = 1,2,3 representing the values of u,v,w respectively, and j = 1,2,3 representing the values for x,y,z respectively.

$$\frac{\partial u_i}{\partial t} + u_j \frac{\partial u_i}{\partial x_j} = g - \frac{1}{\rho}\frac{\partial P}{\partial x_j} + \nu \frac{\partial^2 u_i}{\partial x_j \partial x_j} \tag{2.10}$$

In the RANS-Solver an averaging term is introduced, so that the equation contains some components of the mean flow in the NS-Equation and a fluctuating term, the Reynolds stress tensor. Then the Navier-Stokes equation can be expressed in Cartesian tensor form as follows:

$$\underbrace{\frac{\partial \overline{u_i}}{\partial t} + \overline{u_j}\frac{\partial \overline{u_i}}{\partial x_j} = -\frac{1}{\rho}\frac{\partial \overline{P}}{\partial x_j} + \nu \frac{\partial^2 \overline{u_i}}{\partial x_j \partial x_j}}_{\text{Mean flow NS-equations}} - \underbrace{\frac{\partial (u_i' u_j')}{\partial x_j}}_{\text{Reynolds stress tensor}} \tag{2.11}$$

Where the mean flow are four equations solved for the average values of $\overline{u}, \overline{v}, \overline{w}$ and $\overline{P}$. Reynolds stress tensor is what takes turbulence into account and is solved using different turbulence models. The equation can be rewritten once more, giving:

$$\frac{\partial \overline{u_i}}{\partial t} + \overline{u_j}\frac{\partial \overline{u_i}}{\partial x_j} = -\frac{1}{\rho}\frac{\partial}{\partial x_j}\left[\overline{P}\delta_{ij} + \mu\left(\frac{\partial \overline{u_i}}{\partial x_j} + \frac{\partial \overline{u_j}}{\partial x_i} \right) - \underbrace{\rho u_j' u_i'}_{\text{Fluctuations}} \right] \tag{2.12}$$

The last term solves for the influence of the fluctuations, not the fluctuations themself. This is used to model the effect of turbulence, and do not solve for the eddies in the flow. The last term can be found by several models, such as $k - \epsilon$, $k - \omega$ and $k - \omega SST$.

2.2.4 Turbulence modelling

For the current state of CFD, it is impossible to solve for turbulent flows of practical engineering without invoking turbulence models (Cengel and Cimbala, 2010). There is a variety of turbulence models available for modeling different flow behaviors, depending on the required accuracy of the simulation and the computational capacity. Ranging from fully numerically solved Navier-Stokes equations to a high level of modeling of the influence of the turbulence, the different models will require different computational power. Reynolds-Averaged Navier Stokes (RANS) models the influence from the turbulence, while Direct Numerical Simulation (DNS) solves the equations for turbulent flow directly (Pettersen, 2019). The latter is mostly used in high-end research due to its high computational complexity.

Star-CCM+ offers a variety of turbulence models within the RANS-solver approach to the Navier-Stokes equations, where the main models are $k - \varepsilon$, $k - \omega$, Reynolds Stress Transport and Spalart-Allmaras (CD-Adapco, 2016). Each model got different strengths and weaknesses and are used for different types of simulations. Some turbulence models are optimized for a certain level of y+-values, giving an upper range of applicability for the y+-value depending on the flow physics and the boundary layer profile.

The main turbulence models used in the RANS solution are $k - \omega$ SST and realizable $k - \varepsilon$. Until the last decade of the twentieth century, the $k - \varepsilon$ model was by far the most popular method to simulate the mean flow characteristics for turbulent flow conditions (c. Wilcox, 2006). This

model is a two-equation model and solves the transport equations for the turbulent kinetic energy k and the turbulent dissipation rate ε (CD-Adapco, 2016). There are many various forms of the $k - \varepsilon$ turbulence model optimized for different parameters such as Reynolds number and y+ value. Realizable two-layer $k-\varepsilon$ is often used for added flexibility with an all-y+ wall treatment.

$k - \omega$ is also a two-equation turbulence model that is frequently used. One significant advantage of this model is that it can be applied throughout the boundary layer, including the viscous-dominated region without any modifications. An additional advantage reported for this model is that it has better performance for boundary layers under adverse pressure gradients compared to the $k - \varepsilon$ model (CD-Adapco, 2016).

The $k - \omega$ SST model was developed as an improvement to the two previously mentioned models. The $k - \omega$ SST model address the strengths and weaknesses of $k - \varepsilon$ and $k - \omega$ to improve the model provide better separation prediction. This turbulence model blends a $k - \varepsilon$ model in the far-field with a $k - \omega$ model near the wall (CD-Adapco, 2016). By using an additional cross-diffusion term in the equation, this model ensures that both the near-wall as well as far-field zones are properly resolved (Baek et al., 2015).

2.2.5 Meshing

To solve the governing equations in the computational domain, the domain must be discretized into a mesh. A mesh is a discretized representation of the computational domain where the numerical solution is calculated using the physics solvers. For each cell, the governing equations are solved for the physical process for all time steps.

The grid generation process should be given particular attention since the quality of the results strongly relies on the quality of the grid. Star-CCM+ provides integrated meshing tools that generate high-quality mesh for various geometries and applications. The preferred cell shape used in simulations depends on the particular geometry and solution method used for the particular problem. Some of the standard topologies are shown in Figure 2.5. For practical applications, tetrahedral or hexahedrons are the most used cell shapes (Liseikin, 2010). A combination of different cell types can also be used. Koushan et al. used a combination of hexahedral mesh cells and polyhedral mesh cells for the numerical study of pre-swirl stators. The polyhedral cells were used in the rotating propeller region (Koushan et al., 2020).
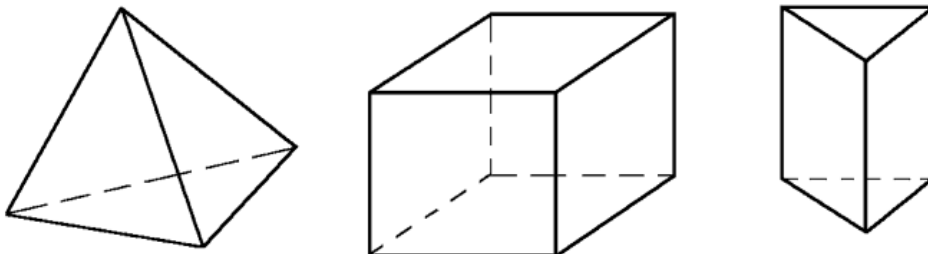
Figure 2.5: Tetrahedon, hexahedron and triangular prism cell (Liseikin, 2010)

The number of cells, thus the cell size, strongly influence the results of the simulation. For a

coarse grid the results will not be realistic, and for a fine grid the simulation require much computational power and computational time. The optimal mesh refinement can be found through convergence studies. One way to perform a convergence study is through a structured approach where different mesh refinements can be tested to see when the results converge, but this is a time consuming process. If experimental data are provided, a less time-consuming method is to perform the convergence study with regard to these data, which was the case for Nowruzi and Najafi's numerical study of different pre-swirl stators on series 60 ships (Nowruzi and Najafi, 2019). For this method, the mesh refinement is increased until the results converge towards the experimental results.

Grid types are divided into two classifications; structured grids and unstructured grids. The main difference of the classes is how the points are located relative to each other, and whether the cells are defined by a general rule. If that is the case, the mesh is considered structured. Some advantages of structured grids compared to unstructured grids, are better convergence and higher resolution. If the connection of the neighboring grid node varies largely from point-to-point the mesh is called unstructured. Unstructured grids have irregularly distributed nodes and the cells do not have to be any of the standard shapes, and thus this class is the most flexible tool for advanced geometry.

Star-CCM+ provides multiple tools to construct the mesh for the entire domain. At solid surfaces, the surface mesher is used, in the boundary layer the prism layer mesher is used and for the main volume in the domain the trimmed cell mesher is used.

2.2.6 Prism layer mesher

The prism layer mesh model is used to generate orthogonal prismatic cells at wall surfaces and boundaries. The prism layers allow the solver to calculate the flow near the surface more accurately. A correctly resolved boundary layer is critical to determine the forces on the walls and at separation points (CD-Adapco, 2016). The mesh should be denser in areas where there are large velocity gradients or other quantities that would strongly affect the flow such as vortex shedding and the flow in the vicinity of the free surface.

The prism layer is characterized by the thickness of the first cell and the total thickness of the boundary layer. The thickness of the first cell on the wall, *hw*, can be calculated from formulas based on the desired y+ value, L_{PP}, Reynolds number, and the friction coefficient, C_F. Δy is half the height of the first cell (Przybylski, 2015). The y+-value is a non-dimensional value used to ensure that the distance from the wall to the first mesh node is small enough for the turbulence model.

$$\Delta y = \frac{y+ \cdot \nu}{u*} = \frac{y+ \cdot \nu}{\sqrt{\frac{\tau_w}{\rho}}} \qquad (2.13)$$

With the wall shear stress, τ_w given as

$$\tau_w = C_F \cdot \frac{1}{2}\rho \cdot U_\infty^2 \qquad (2.14)$$

$$\Delta y = \frac{y+ \cdot \nu}{\sqrt{C_F \cdot \frac{1}{2}U_\infty^2}} = \frac{y+ \cdot \nu}{U_\infty \sqrt{\frac{C_F}{2}}} = \frac{y+ \cdot L_{PP}}{Re \cdot \sqrt{\frac{C_F}{2}}} \qquad (2.15)$$

The friction coefficient can be found using ITTC-57s equation.

The thickness of the prism layer should contain the entire boundary layer, but there are two issues with this; the boundary layer does not have a definite boarder, and more importantly, the exact boundary layer is not known before the CFD-solution is ready. This means that the boundary layer thickness must be found analytically or through an iterative process.

2.2.7 The trimmed cell mesher

To generate the volume mesh in the domain, the trimmed cell mesher can be used. The trimmed cell mesher offers a robust and efficient method to generate a high-quality mesh for complex geometries (CD-Adapco, 2016). The trimmed mesher combines several desirable meshing attributes such as hexagonal cell topologies, alignment with user-specified coordinate system, and ability to trim the core mesh so that it can accommodate complex geometries. This typically results in a mesh of good quality with a high degree of orthogonality in the free stream flow. By including volumetric controls, the mesh density can be increased or decreased locally to ensure optimal mesh refinement in the critical areas. This mesher removes the cells that are overlapping with the geometry.

2.2.8 Free surface modeling

To model free surface flow in STAR-CCM+ the Volume of Fluid, VOF, model is used. This model is used when simulating surface gravity waves on the interface between a dense fluid and a light fluid, such as water and air (CD-Adapco, 2016). For marine applications, the VOF model is typically used with the 6-DOF Motion model, allowing the ship to move in the water. VOF is a simple multi-phase model, well suited to simulate flows of immiscible fluids. The volume fraction is defined as the ratio between the volume occupied by the phase, over the total cell volume.

2.3 Challenges with CFD

Although the computational power has increased significantly over the last decades making it possible to perform analyses with finer mesh grids and accurate results, there are still some challenges for numerical calculations.

One of the problems in today's CFD calculations is how to include the turbulence in the simulations. The current state of CFD can quite accurately handle laminar flows, but turbulent flows are still impossible to solve without involving simplified models. For industrial level of research, RANS-solvers are used, and this solver does not calculate the turbulence accurately but rather model the influence of the turbulence. The CFD results are therefore highly dependent on the accuracy of the turbulence model. It is possible to solve the Navier-Stokes equations using Direct Numerical Simulations that include the turbulence in the simulations, but currently these simulations are only used for high-end research since DNS is highly computational demanding

(Peric and Bertam, 2011).

Another aspect where the computational power is of interest is in the grid refinement. Preferably, the simulations would be run with a very fine mesh, but that would require significant computational power. The results are greatly influenced by the mesh refinements of the simulation, so it is crucial to run the simulations with an adequate grid. If the grid is too coarse, the software will interpolate between the cells, and this might alter the results in the critical areas. Thus, the grid generation must be done carefully and use finer grids in critical areas, and coarser grids further away from the body.

A problem when meshing with different mesh refinements in the domain is that the cell size varies throughout the domain. Variation in cell size may lead to an issue when the time step Δt is decided. The time step has to be low enough for the time integration scheme so that the fluid flow through the cells are captured. An indication of whether the time step is small enough is the Courant-Friedrichs-Lewy number given in Equation 2.16. For values of CFL-number smaller than one, the distance traveled by the fluid is smaller than the length of the cell, indicating that the time step is small enough. For large values of the CFL-number, the simulation produces incorrect results. u_x is the velocity in x-direction, Δx is the cell size, and Δt is the time step.

$$CFL = u_x \frac{\Delta t}{\Delta x} < 1 \tag{2.16}$$

An additional challenge of CFD is that CFD is highly complex and requires sufficient knowledge and competence from the user. The software provides numerous functions to help users solve complex tasks, but in some cases, these functions are used as black boxes, meaning that the user does not know what the code executes behind the user interface. Commercial CFD-software is not open code sources, which makes it hard to know which models and simplifications are used in the code. Thus, use of CFD-software requires experience and understanding of the physical phenomena that are simulated. This requires a significant amount of hours of training and failure, so the user should show great caution when evaluating the results from the simulations.

Chapter 3

Optimization of pre-swirl stators

3.1 Energy saving devices

There are many devices that can be used to improve the energy performance of new ships and operating ships. Examples of such devices are pre-swirl devices, post-swirl devices, high-efficiency propellers, wake equalizing, and flow separation devices (ABS, 2013). This section explores the working principle of energy saving devices, ESD's, and how to reduce the energy losses of the propeller. Then the principles of optimization of pre-swirl stators will be discussed. Parts of the theory presented in this chapter originates from the project thesis on energy saving devices carried out during the fall of 2019 (Johansen, 2019).

3.1.1 Energy losses

The energy losses of a propeller can be divided into four main classes; momentum losses, rotational losses, frictional losses, and hull interaction losses (Koushan, 2018). Parts of these energy losses can be recovered by careful design or by introducing energy saving devices.

The largest energy loss component is the momentum loss factor. These energy losses are unavoidable but can be decreased in the design process. The momentum loss can be reduced by maximizing the propeller diameter but are often limited by the draft or restrictions for the propeller diameter.

The rotational losses are related to lost kinetic energy in the tangential and swirling velocities in the slipstream of the propeller (Koushan, 2018). These losses can be decreased by mitigating slipstream swirls through introduction of one or more energy saving devices. A pre-swirl device may counteract the swirls, whereas a post-swirl device will convert the swirling velocities into axial velocity.

There are also frictional losses caused by the frictional resistance on the propeller blades and other propulsor components. This component is significant for propellers of high rotational velocity. Adding additional devices, such as ESD's, to the ship would in fact increase the frictional losses even more.

Hull interaction losses originate from the interaction between the hull and the propeller. Hull interaction leads to an inhomogenous wake, and thus decrease the propeller efficiency. With large velocity differences through the propeller disk, the propeller can not work optimally throughout the entire revolution. Inhomogeneous wake also leads to problems regarding cavitation and vibrations on the propeller. Pre-swirl devices and ducts can be designed to change the inhomogeneous wake to a more even wake (Koushan, 2018).

3.1.2 Working principles of ESD's

Energy saving devices are devices designed to optimize the flow to, around, or behind the propeller. ESDs can be fitted for new-builds or added to retrofit an operational vessel. Different energy saving devices are evaluated on their contribution to the reduction of energy losses discussed in Section 3.1.1. Energy saving devices reduce energy losses in various ways such as through reduction of kinetic energy losses, hull-propeller interaction losses, rotational energy losses, or wake equalization. The energy saving devices are located in three schematic zones; in front of the propeller, on the propeller or behind the propeller. (Carlton, 2007). In Figure 3.1 these three stages are defined as Zone I, II and III, respectively.
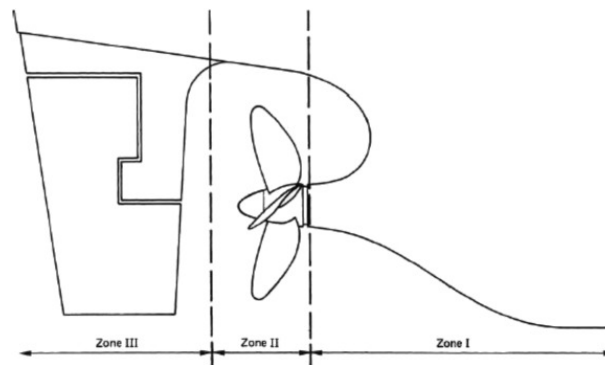
Figure 3.1: Zones to locate ESDs in the stern vicinity (Carlton, 2007)

Table 3.1 gives an overview and examples of ESD's in the three positions, and how they act on the flow to reduce the energy consumption of the ship. The table is created as a summary from Carlton descriptions of energy saving devices in various positions relative to the propeller (Carlton, 2007). The energy saving devices should reduce at least one of the energy losses, but some ESD's can improve the flow in multiple ways. Energy-savings up to 6% have been reported for some ESD's (ABS, 2013). The achieved energy-saving depends on many different factors, such as hull lines, propeller loading and the operational profile of the ship.

Table 3.1: Working principles of ESD's in different zones

Position	Examples of ESD	Working principles
Zone I	Pre-swirl stators, wake equalizing duct, spoilers, stern tunnels.	Manipulate flow into propeller to improve the overall efficiency by creating a more uniform wake and to reduce the tangential velocities.
Zone II	Propeller duct, propeller with end-plates, Grim Vane Wheel	Reduce the energy losses associated with propeller hub vortices, losses from propeller rotation, or convert slipstream energy to additional thrust.
Zone III	Rudder bulb, thrusting fins, boss cap fins	Prevent flow separation and excessive vorticity behind the hub or produce additional thrust from tangential component V_θ in the slipstream.

3.1.3 Device Compatibility

Although individual devices could offer energy savings up to 6%, the combined energy-saving by applying multiple devices cannot be estimated by aggregating the individual savings for each device. Use of one energy saving device might exclude or reduce the efficiency of another device. However, several of the energy saving devices can be used in combination to gain additional energy-savings.

The effect of applying multiple ESD's simultaneously must be carefully analyzed. Not all energy saving devices are compatible with each other as some devices might alter or remove the flow regimes the other devices work in. Compatibility of multiple ESD's must therefore be verified using model tests or CFD analysis. Figure 3.2 shows which of the energy devices that are theoretically fully or partially compatible with each other.

Device compatibility matrix (columns, left to right):
Wake-equalizing, Flow Separation Alleviating Devices: Grothues Spoilers, Schneekluth Ducts, Stern Tunnels — Pre-swirl Devices: Pre-swirl Fins and Stators, Mitsui Integrated Ducted Propeller, Hitachi Zosen Nozzle, Sumitomo Integrated Lammeren Duct, Becker Mewis Duct — Post-swirl Devices: Rudder Thruster Fins, Post-swirl Stators, Assymmetric Rudders, Rudder (Costa) Bulb, Propeller Boss Cap Fit (PBCF), Divergent Propeller Caps, Grim Vane Whels — High-efficiency Propellers: Large Diamter/Low RPM, Controllable Pitch Propellers (CPP), Ducted Propellers, Propellers with End Plates, Kappel Propellers, Contra-rotating Propellers, Podded and Azimuthing Propulsion — Skin Friction Reduction: Air Cavity Systems, Micro Bubbles — Renewable Energy: Towing Kites, Flettner Rotors, Windmills, Turbosail

Wake-equalizing, Flow Separation Alleviating Devices

Device	Pre-swirl	Post-swirl (RTF–GVW)	High-efficiency	Skin Friction	Renewable
Grothues Spoilers		C C C C C C C	C PC · C C C	C C	C C C C
Schneekluth Ducts		C C C C C C C	C PC · C C C	C C	C C C C
Stern Tunnels	C PC PC PC PC	C C C C C C C	C C · C C C	C C	C C C C

Pre-swirl Devices

Device	Post-swirl (RTF–GVW)	High-efficiency	Skin Friction	Renewable
Pre-swirl Fins and Stators	C C C C C C	C PC C · C C	C C	C C C C
Mitsui Integrated Ducted Propeller	C C C C C C C	C PC · PC PC	C C	C C C C
Hitachi Zosen Nozzle	C C C C C C C	C PC · C C	C C	C C C C
Sumitomo Integrated Lammeren Duct	C C C C C C C	C PC · PC PC	C C	C C C C
Becker Mewis Duct	C C C C C C C	C PC · PC PC	C C	C C C C

Post-swirl Devices

Device	Post-swirl	High-efficiency	Skin Friction	Renewable
Rudder Thruster Fins	C C C	C PC PC C C	C C	C C C C
Post-swirl Stators	C C C	C PC C C C	C C	C C C C
Assymmetric Rudders	C C C	C PC C C C	C C	C C C C
Rudder (Costa) Bulb	C C	C C C C C PC	C C	C C C C
Propeller Boss Cap Fit (PBCF)		C C C C C	C C	C C C C
Divergent Propeller Caps		C C C C C PC	C C	C C C C
Grim Vane Whels		C · PC PC · PC	C C	C C C C

High-efficiency Propellers

Device	High-efficiency	Skin Friction	Renewable
Large Diamter/Low RPM	C · PC PC C	C C	C C C C
Controllable Pitch Propellers (CPP)	C C C	C C	C C C C
Ducted Propellers	PC PC C C	C C	C C C C
Propellers with End Plates	C	C C	C C C C
Kappel Propellers	C	C C	C C C C
Contra-rotating Propellers	C	C C	C C C C
Podded and Azimuthing Propulsion		C C	C C C C

Skin Friction Reduction

Device	Renewable
Air Cavity Systems	C C C C
Micro Bubbles	C C C C

Renewable Energy

| Device |
|---|
| Towing Kites |
| Flettner Rotors |
| Windmills |
| Turbosail |

LEGEND
- C — The devices are theoretically fully compatible with each other
- PC — The devices are partially compatible and overall efficiency is not fully additive

Figure 3.2: Device Compatibility (ABS, 2013)
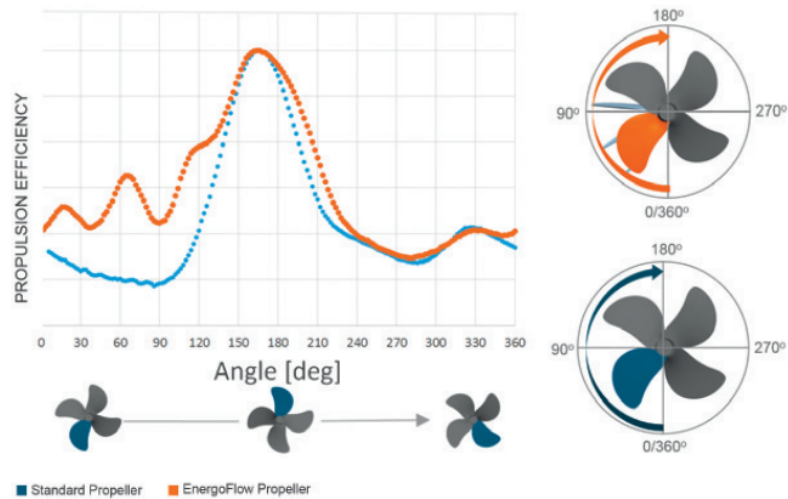
3.1.4 Pre-swirl stators

Pre-swirl stators, PSS, are a type of pre-swirl device located in front of the propeller. The number of fins can vary, but there are usually three to five fins. The fins manipulate the flow into the propeller in the opposite direction of the propeller rotation to create a more homogeneous wake. That means that for a right-hand propeller, the fins will be placed at the port side of the stern, and for a left-hand propeller, the fins are placed at the starboard side of the stern. Stator fins can be designed to improve the flow of both existing ships and new-builds. In general are pre-swirl stators compatible with all ship types, ranging from bulkers, container ships, RORO's and gas carriers (ABS, 2013). Pre-swirl stators have shown to deliver energy-savings of 4%-6% at self-propulsion depending on the conditions of the ship (Koushan et al., 2020), (ABS, 2013). Figure 3.3 show an example of a pre-swirl stator with a small nozzle ring to improve strength. The figure illustrates how the stator fins redirect the flow into the propeller in the opposite direction to the propeller rotation.
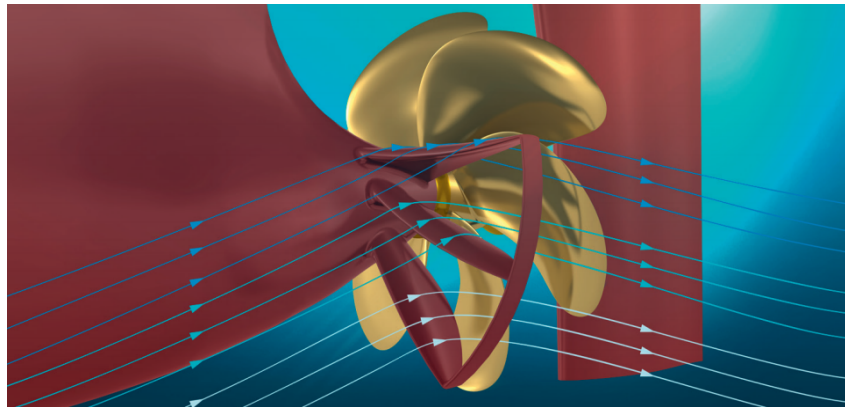
Figure 3.3: Pre-swirl stator (Wärtsilä, 2017a)

The PSS serves a multipurpose by both breaking up vortices due to separation in the stern region and redirecting the flow into the propeller to equalize the wake. The pre-swirl stator's purpose is to optimize the wake at the propeller plane so that the propeller blades are more heavily and uniformly loaded (van Terwisga, 2013). When the relative velocities are altered, the rotation rate of the propeller can be reduced since the propeller blades will experience the same effective angle of attack. A reduction of rotational speed on the propeller will decrease the energy consumption of the ship. Since the PSS is a passive fin system, it does not improve the overall efficiency of the propulsor-ship system by creating thrust, but can rather decrease the rotational kinetic energy losses and thus increase the axial kinetic energy and momentum flux, and thus increase the thrust (van Terwisga, 2013). Implementation of a PSS will also modify the torque since the propeller blades are more heavily loaded. This allows for a reduction of the propeller rotational velocity at equal thrust, which in turn also reduces the friction losses of the propeller.

The pre-swirl stator alters the transverse nominal wake of the propeller so that the relative velocities to the propeller blade differ less during one revolution. With reduced velocity differences, it possible to design a propeller with increased efficiency over the revolution. Figure 3.4 shows how the propeller efficiency is increased when a pre-swirl stator is used, and this leads to energy savings for the system.

Figure 3.4: Propeller efficiency with and without use of pre-swirl stator (Wärtsilä, 2017b)

3.1.5   Propeller boss cap fins

A propeller boss cap fins, PBCF, is an example of an energy saving device behind the propeller. PBCF are devices that can be used alone or in combination with other ESDs such as pre-swirl stators. The PBCF is designed to prevent flow separation and excessive vorticity behind the hub of the propeller. When properly designed for the propulsion system, the PBCF may produce additional lift force to the system. Propeller boss cap fins can be implemented in combination with a pre-swirl stator to provide additional energy savings (Koushan et al., 2020). When using only a pre-swirl stator there is still considerable kinetic energy downstream of the propeller, and this can be utilized by a PBCF. An optimization study of PSS and PBCF combined could be of interest, since this may lead to additional energy-saving for the system.

Since 1987 there has been a significant amount of research of the effect of the propeller boss cap fins both numerically and experimentally for model scale and full scale. A large number of PBCFs have been installed on all types of ships such as tankers, including VLCC, Container, PCC, and ferries. Nojiri et al. analyzed the result for full-scale analyses for 16 different vessels and found that the PBCF has an energy-saving effect of 2 to 10%, with an average of 5% (Nojiri et al., 2011). These results are considerably higher than what is found for model scale and full scale with use of numerical calculations.

Kawamura et al. carried out CFD analyses of propeller boss cap fins at model and full scale Reynolds numbers with the intention of finding out why the energy-saving values are so much higher for full scale than for model scale. The results of computations at different conditions shows that increased Reynolds number and presence of hull wake both positively influence the effects of PBCF. Due to the combined effect of the Reynolds number and the wake, the gain in the propeller efficiency at the full-scale condition was found to be significantly larger than that at the model test condition. For full-scale condition, the fin drag becomes smaller, and the reduction of the boss drag becomes larger. The predicted gain is however smaller than the values reported in the sea trial and logbook analysis, and the remaining gap can be caused by interaction between hull and rudder, or the surface roughness of the ship (Kawamura et al., 2012). The

results of this report seems a little high, but it set focus on the issue of full-scale analysis since it shows that the model scale results are quite far off from the logbook analysis.

Sun et al. performed a numerical and experimental study on the energy-saving of propeller boss cap fins with the rudder included in the system and to see how the PBCF impact the hydro-dynamic performance of rudders. Hydrodynamic experiments were carried out on propeller-rudder systems with PBCFs in a cavitation tunnel. The experimental energy-saving effect of the PBCF without a rudder was 1.47% at the design advance coefficient J=0.8. This study state that the PBCF increase the resistance on the rudder due to an increased pressure at the leading edge, which results in a reduction in the over-all energy-saving effect of the PBCF. When the rudder is included in the system, the energy-saving effect decrease from 1.47% to 1.08% for an ordinary rudder, and 1.16% for a twister rudder, this implies the importance of including the rudder in the propulsion system when evaluating the energy-saving effects of PBCFs (Sun et al., 2016).

(a) Propeller without PBCF   (b) Propeller with PBCF
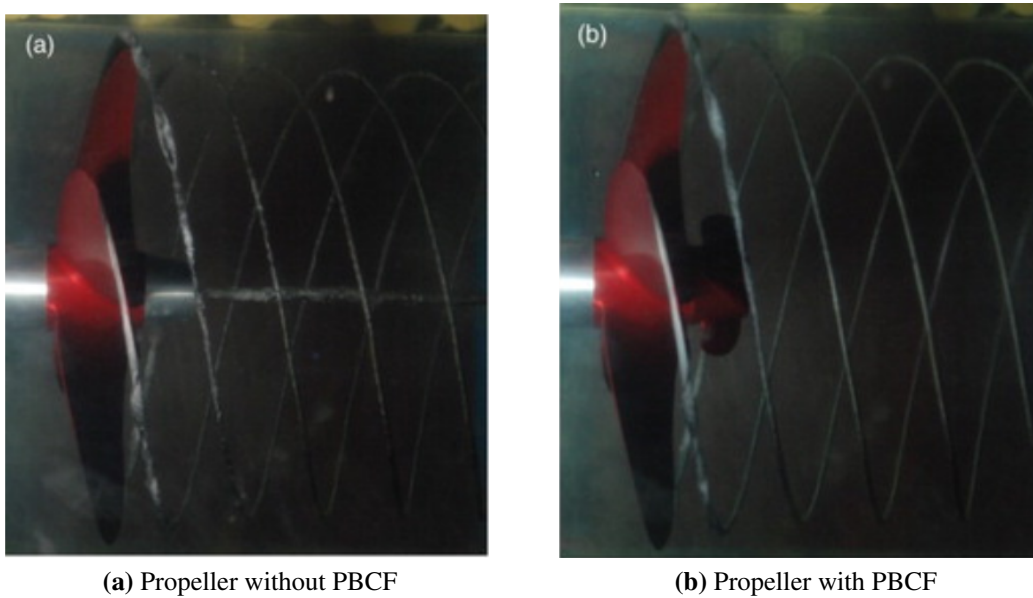
Figure 3.5: Influence of PBCF (Sun et al., 2016)

3.2   Pre-swirl stator optimization

3.2.1   Design considerations

There are several design apects to take into consideration during the design process of a pre-swirl stator. Koushan et al. states that the shape of the fins should be designed to maximize the desired effect of the pre-swirl, and at the same time, minimize the separation, vortex shedding and the strength of the tip vortex on the fins (Koushan et al., 2020). That means that each fin should be designed to have the optimal pitch and camber along the span to give the optimal flow features. When designing the PSS, it may be preferred to create a neutral PSS in terms of axial force contributions and focus on the optimization of the flow into the propeller. A neutral PSS means that fins are not designed to provide thrust to the system, but rather focus on improving the efficiency of the propeller. Neutral PSS decreases the risk of giving an adverse effect on the flow over the stern.

When exploring different designs for the pre-swirl stator, there are some geometric parameters that should be studied (Koushan et al., 2020). These parameters include fin geometry parameters, such as fin radius, thickness, chord length, and pitch angle, as well as fin installation parameters such as the position of PSS plane, number of fins, position of the fins, and fin installation angles should also be studied. Since a full optimization of all these parameters requires considerable CPU time, only fin radius, angular position, and pitch angle are to be considered in this thesis.

There are several phenomena that are essential to take into account in the design phase. To make sure that the interaction phenomena between the hull, propeller, PSS, and rudder are taken into consideration, the propeller must be implemented as a rotating propeller and not an actuator disk. The optimization should also be performed in full-scale since Reynolds number is higher for full-scale ships compared to model-scale. Different Reynolds number leads to a different boundary layer, and the velocities distribution in the wake will not be similar (Regener et al., 2018). This makes CFD is an efficient and powerful tool to analyze the performance of pre-swirl stators since full-scale ships can be studied in detail (Koushan et al., 2020). Through CFD-simulations, it is possible to analyze the velocities in the propeller slipstream, and that way, give an insight into the performance of the PSS.

3.2.2   Optimization method

The optimal configuration of the pre-swirl stator is found from a comparison of the results for different variations of the parameters radius, angular position, and pitch angle. There are two adequate objective functions that could be used to quantify the efficiency of an ESD for a given ship. One way is to maximize the increase of propulsive efficiency, and the other is the maximize the achievable reduction of the shaft delivered power, PD. Since the simulations will be performed with a fixed propeller rotational speed, the first objective function will be used for this thesis. The increase in propeller efficiency is calculated as derived in Equation 3.1. In this equation, η_{PSS} and η_S is the propeller efficiency with and without implemented PSS, respectively. By comparing the increase in propeller efficiency, $\Delta\eta_P$, it is possible to decide which parameter configuration that gives the largest energy saving. The wake field is also interesting to compare since this can expose changes in the axial and transverse velocities

at different sections of interest, thus also expose changes the axial and transverse kinetic energy.

$$\Delta\eta_P = \frac{\eta_{PSS}}{\eta_S} = \frac{\frac{T_{PSS} \cdot V}{PD_{PSS}}}{\frac{T_S \cdot V}{PD_S}} = \frac{\frac{T_{PSS}}{PD_{PSS}}}{\frac{T_S}{PD_S}} \qquad (3.1)$$

To find the optimal configuration of design parameters for the pre-swirl stator various combinations are investigated. By varying one parameter at a time, the results could be compared to see which configuration that gives the largest energy saving. Once the optimal configuration for one parameter is found, this is used for the remainder of the simulations. This is the same approach that is used by Kim et al. and is used to save considerable time and computational effort (Kim et al., 2013). This method does not take the coupling between the parameters into account like a formal optimization method, such as particle swarm optimization, would.

All the variations of the design parameters are summarized in Table 3.2. The optimization process starts with finding the optimal fin radius, then the angular position, and at last, the optimal pitch angle of the fins.

3.2.3 Radius of stator fins

The influence of the radius of the stator fins will be investigated by varying the radius from the initial configuration. The initial configuration has a radius equal to 1.077R of the propeller diameter. When varying the radius of the stator fins, it is essential to investigate if the resistance increase from the fins (Kim et al., 2013). The PSS is investigated at radius values of 1.10R, 1.077R, 1.05R, 1.00R, and 0.90R. The radius that gives the best results will be used for the optimization of the angular position and pitch angle. Figure 3.6 show the interval of which the fin radius is varied. Only one fin radius smaller than the propeller radius is investigated since the flow in the stern area contracts due to the hull shape.
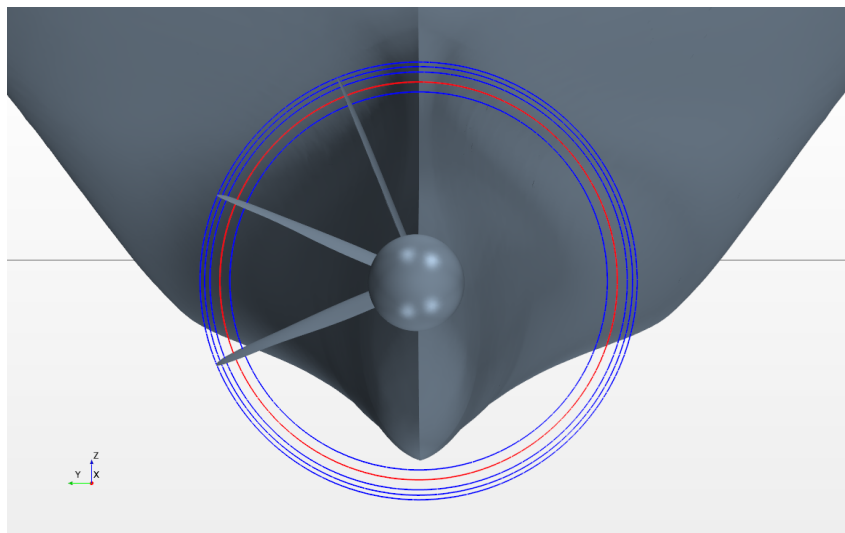

Figure 3.6: The radius of the fins are varied between 0.9R to 1.1R. The radius in red corresponds to the propeller radius.

3.2.4 Angular position of stator

Next step of the optimization process is to find the optimal angular position for each of the stator fins. By adjusting the angular position of the stator fins, the flow field will be altered, and the hydrodynamic performance of the propeller might improve. By systematically adjusting the angular position of each fin the optimal position can be found. Each of the fins is rotated relatively to the initial set-up one blade at a time, starting with the lower fin, with positive direction counter clockwise. The lower, middle, and upper fin is adjusted ± 5 degrees from the initial position at 113, 67 and 22 degrees from the z-axis respectively. All angular configurations investigated are given under *Angular position* in Table 3.2. Figure 3.7 shows how the stator fins rotate relative to the original position.
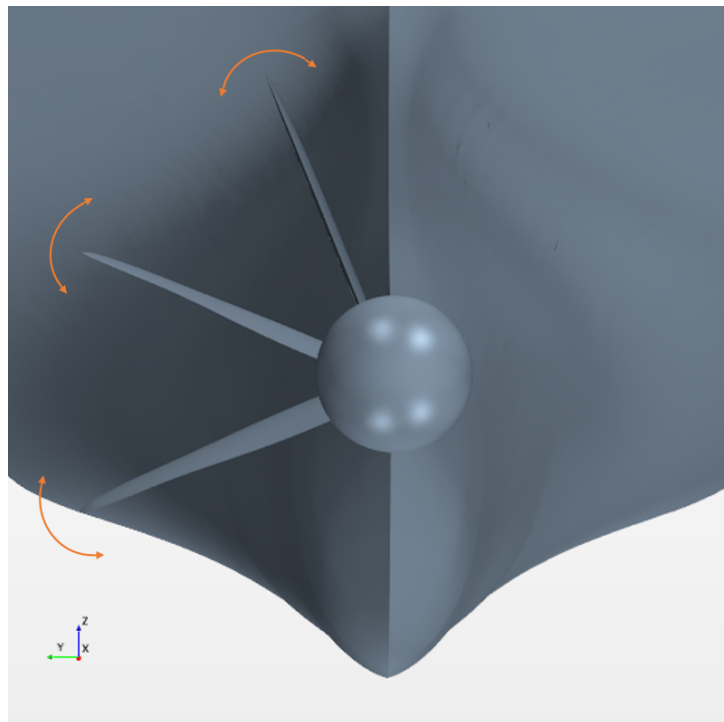
Figure 3.7: How the fins are rotated. Positive direction is defined counter clockwise.

3.2.5 Stator pitch angle

The stator pitch angle plays an important role in the redirection of the flow into the propeller. How the flow enters the propeller influence the efficiency of the propeller, and an improved flow field will increase the hydrodynamic performance of the propeller. The stator fins are rotated about its axis along the length of the fin. All fins are rotated at once, with increments of 4 degrees from the initial position at 91.0, 77.5, and 68.0 degrees for the upper, middle and lower fins, respectively.

When finding the optimal stator pitch angle, the increase in propeller efficiency is compared for the different configurations. It is also interesting to investigate the distribution of transverse velocities into the propeller. By varying the stator pitch angle, the angle of attack on the propeller may be improved, and the efficiency of the propeller increase. It is also important to keep in mind that changing the pitch angle might increase the resistance due to drag.

3.3 Optimization parameters

Table 3.2 gives an overview of the different configurations that are investigated for the design parameters of the pre-swirl stator. 15 alternative solutions are evaluated to maximize the objective of maximizing the propeller efficiency. The results from the simulations are presented in Chapter 5.

Table 3.2: PSS configurations investigated in the design parameter variation study

Optimization parameter	Simulation No	Upper	Middle	Lower	Remarks
Fin radius	1	1.10R	1.10R	1.10R	R is radius of propeller
	2	1.077R	1.077R	1.077R	Initial configuration
	3	1.05R	1.05R	1.05R	
	4	1.00R	1.00R	1.00R	
	5	0.90R	0.90R	0.90R	
Angular position	6	22	67	108	Degrees from z-axis
	7	22	67	113	Initial configuration
	8	22	67	118	
	9	22	62	108	
	10	22	72	108	
	11	18	67	108	
	12	27	67	108	
Pitch angle	13	83.0	69.5	60.0	
	14	87.0	73.5	64.0	
	15	91.0	77.5	68.0	Initial configuration
	16	95.0	81.5	72.0	

Chapter 4

Numerical set-up

This chapter presents the settings that are utilized for the numerical set-up. Star-CCM+ provide multiple models for the numerical calculations so that the physical problem should be simulated correctly. To investigate the how pre-swirl stators influence the hydrodynamic forces and the wake field of a propagating ship, the the right physical models must be implemented in the computational domain. The software used for the simulations is Star-CCM+, which is a full range CFD software provides models for all parts of the simulation process.

4.1 Problem set-up

The numerical simulations are performed for a chemical tanker with L_{PP} = 175.6m, and are performed in full scale so that the wake will be similar to the real ship. The results from the simulation are compared to Koushan et al.s numerical results for the same ship to evaluate the numerical setup (Koushan et al., 2020). The set-up for the simulation is influenced by Koushan et al.s CFD set-up for their study on pre-swirl stators in Star-CCM+.

The simulated ship velocity is set to be at the ship's design velocity of 14 knots, corresponding to 7.2016 m/s. Simulations are performed at design draught at 11.846m, and propeller rotational speed of 1.472 rps. More of the main ship parameters are given in Table 4.1.

Table 4.1: Main ship and propeller parameters

	Symbol	Value
Length between perpendiculars	L_{PP}	175.60 [m]
Breadth moulded	B	32.229 [m]
Draught	T	11.846 [m]
Block coefficient	C_B	0.8123
Ship velocity	V_S	7.2016 [m/s]
Propeller diameter	D	6.5 [m]
Rotational speed	n	1.472 [1/s]
Number of blades	Z	4
Direction of rotation	-	Right-handed

The simulations are performed using two different domains; one with free surface and one using double-body model. Double-body model means that the ship's hull is reflected with a symmetry plane at the waterline at rest, and the flow around the hull will be as it would in an undeformed water surface without waves (Bertram, 2011). Using a double-body model gives faster convergence, and thus shorter computational time. The difference between the resistance of the

double-body model and the free surface simulation will be accounted as the wave making resistance and will be added to the ship resistance without free surface when comparing the results to the experimental data. Although it is known that the ESDs might affect the wave making drag, this effect is considered limited and will be neglected in the simulations (van Terwisga, 2013).

When the wave making resistance is found, the rest of the simulations are executed in the domain without free surface. The resistance is found using the naked hull with rudder and then the propeller is implemented later. For the simulations considering the pre-swirl stator a rotating propeller is implemented so that the interaction between the hull, PSS, rudder and propeller is taken into account.

The initial PSS is introduced when the set-up is verified. The simulations for the optimization study are performed in two steps; first using moving reference frame, MRF, then followed by rigid body motion, RBM. This is two-stage process is performed to provide an initial condition for the RBM-model. Rigid body motion approach gives accurate results to this problem but it a remarkably computational demanding model. Using a steady-state technique therefore gives satisfactory initial values and will save a significant amount of time for each configuration since the RBM-solver only have to be run for a short period until the results converge to a quasi-steady state.
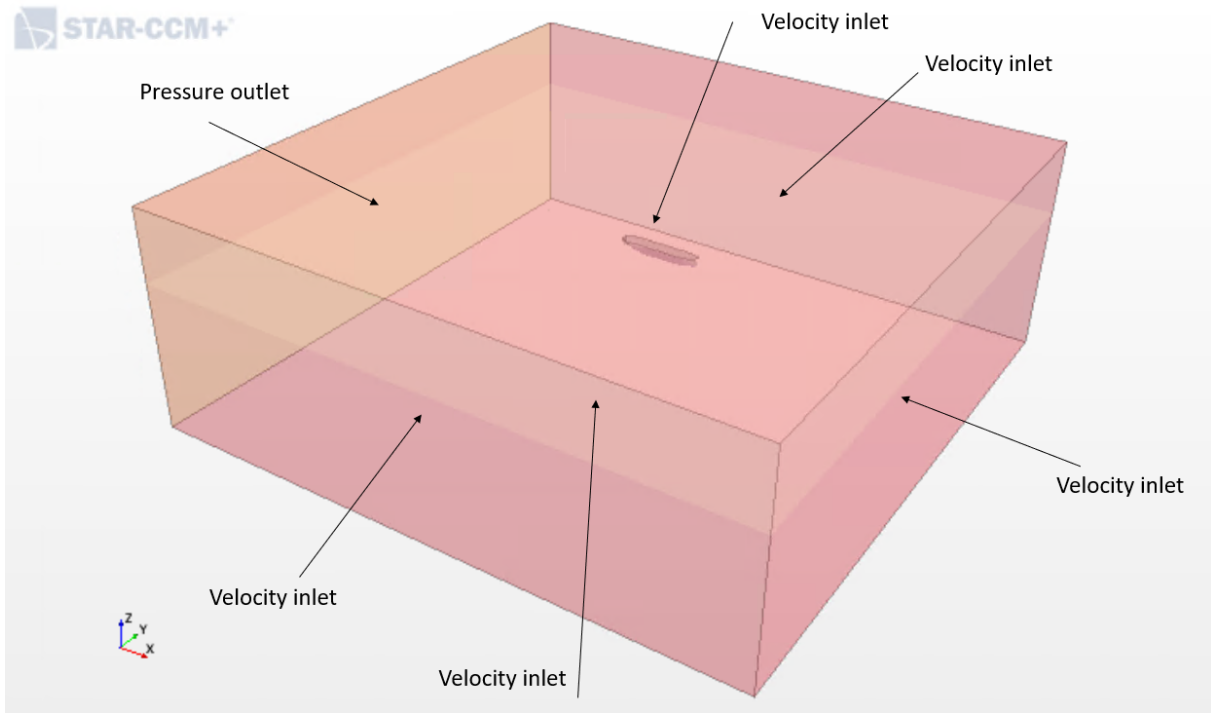
4.1.1 Domain

To keep the cell count in the domain to a reasonable level, the dimensions of the computational domain must be set as small as possible while still accounting for the influence from the boundaries on the flow around the vessel. Table 4.2 show the dimensions used for the domains in the simulations with and without free surface, respectively.

Table 4.2: General domain parameters with and without free surface

| General domain parameters	With FS	Without FS
Length between perpendiculars L_{PP}	175.60 [m]	175.60 [m]
Inlet position	-4 $\cdot L_{PP}$	-4 $\cdot L_{PP}$
Outlet position	4 $\cdot L_{PP}$	4 $\cdot L_{PP}$
Sides	$\pm 2 \cdot L_{PP}$	$\pm 2 \cdot L_{PP}$
Top	1 $\cdot L_{PP}$	Draught
Bottom	-2 $\cdot L_{PP}$	-2 $\cdot L_{PP}$

The domains with and without free surface have deviating boundary conditions due to different simulation environments. Similar for both domain is that the inlet, bottom and sides are modeled with velocity inlet, and the outlet is modeled with pressure outlet. For the domain with free surface is modeled as velocity inlet, and in the domain without free surface the top region is modeled as symmetry plane. Figure 4.1 shows the boundary conditions for the different regions in the domain with free surface. For the free surface simulations, free surface damping function was enabled at the boundaries of the virtual towing tank to avoid the wave reflections.

Figure 4.1: Domain with applied boundary conditions for free surface simulations

4.1.2 Meshing

To maintain good results while keeping the cell count low, the mesh is generated so that there is a finer in areas where there are expected large changes in the gradients. Figure 4.2 shows that the cell size is coarse in the the domain, but that it becomes finer closer to the ship. This apply to the area close to the hull, and especially near the bulb and aft of the ship. The region close to the hull is subject to several mesh refinements, so that there is a smoother transition to the coarser volume mesh. Trimmed mesher is used to create the mesh for the main fluid region, containing the ship hull, rudder and PSS. This gives mainly a hexahedral mesh, with trimmed cells at the wall surface of the input geometries. In the rotating region enclosing the propeller, a polyhedral mesh is generated.
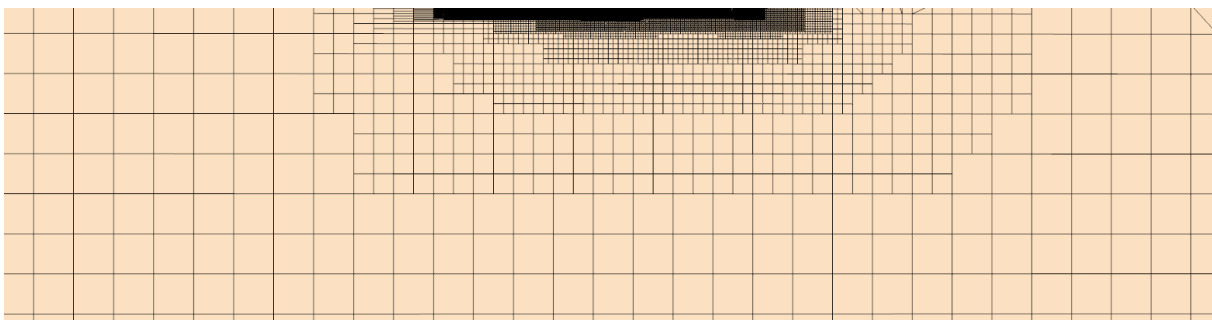
Figure 4.2: Mesh configuration in the domain

Figure 4.3 shows the details of the mesh configuration aft of the ship. The mesh is significantly finer at the skeg to capture bilge vortices since these will interact with the PSS and influence the flow into the propeller. In the figure, the interface between the rotating domain and the fluid domain can be seen as the square around the propeller. The fluid domain and the rotating domain are set up as two individual regions with individual mesh refinements and motion specifications.
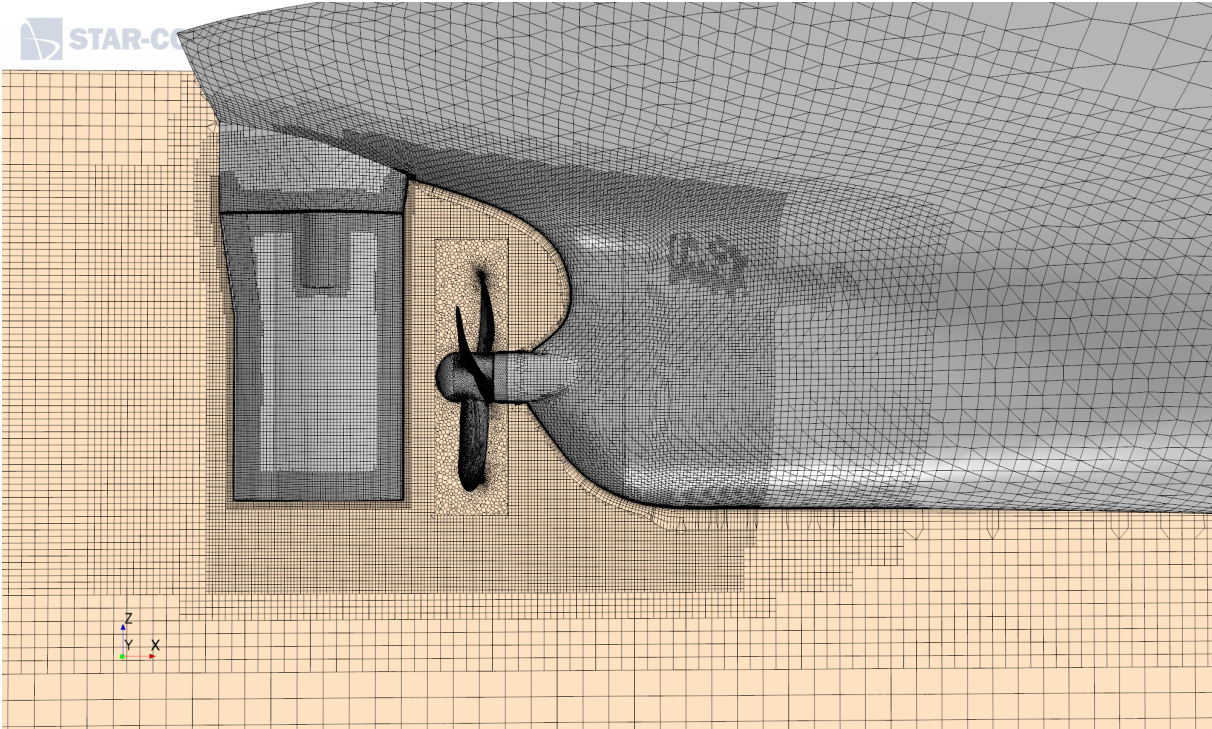
Figure 4.3: Details of the mesh configurations

Prism layer mesh is generated at the wall boundaries of the geometries to resolve the velocity profiles in the boundary layer. The near-wall thickness and boundary layer thickness is set to meet the desired wall Y+ levels. To reduce the computational effort, it is aimed to keep the Y+-value is lowest at the most critical areas and higher for less critical areas. At the hull, the averaged target Y+ values are 150, and 70 at the rudder and 30 at the propeller blades. Figure 4.4 shows the Y+ distribution at the different parts of the hull.

Figure 4.4: Y+ value at different parts of the hull

4.1.3 Simulation set-up

Star-CCM+ provide many different models to make the simulations provide as correct physical settings as possible for the specific physical environment. Central settings for the numerical calculations are choice of turbulence model, time step, physics models, and motion settings. Table 4.3 summarize some of the central CFD settings used for the simulations in the optimization process. The simulations of the chemical tanker are completed using Star-CCM+ version 15.02.007.

Incompressible RANS equations are used to solve the governing equations in the domain, and $k - \omega$ SST is used to model the turbulence. Realizable $k - \varepsilon$ was also investigated but did not attain the desired results. The $k - \omega$ SST model solves flow near the walls of the body as well as the wakefield. An All y+ wall treatment model was used.

Table 4.3: CFD settings used in the simulations

Analysis condition	Setting
Software	Star-CCM+ Version 15. 02.007
Governing Equation Model	Incompressible RANS equation
Turbulence Model	$k - \omega SST$
Wall Treatment	All y+ wall treatment
Time solver	Implicit unsteady
Temporal discretization	2nd-order
Rotation Method	Rigid body motion

The free surface was simulated using the volume of fluid, VOF, multi-phase model. The calculations are performed with a fixed ship, so that the model does not have the ability to move in heave and pitch. This is based on the assumption that the ship will not have large motions in heave and pitch and is done to save computational time.

The simulations used to compare the different versions of pre-swirl stators are run without use of free surface. For these simulations, instead of a free surface, the domain is modeled with a symmetry plane where the free surface would have been. Similar as for the free surface simulation, there is not implemented any trim to the vessel, so the symmetry plane is set at the design draught of the ship.

When the rotating propeller is implemented, the time step is set to be corresponding to a two-degree rotation of the propeller. So the time step for the is calculated to be 1/180th of the propeller rotational speed. When the rigid body motion for the propeller is applied, the temporal discretization property is set to be second-order implicit unsteady. Second-order temporal discretization is found to give more accurate results than first-order (CD-Adapco, 2016).

Figure 4.5 shows some of the relevant plane sections for the simulations. The plane sections are called 'Propeller plane' 'Inflow' and 'ESD plane' when they are mentioned later. The origin of the 'Propeller plane' is in the center of the propeller and indicates where the coordinate system of the in the propeller is. The second plane section is 'Inflow plane'. This section is when investigating the velocity flow into the propeller, and is located 0.65m upstream of the propeller plane. This plane is used to avoid singularities, which might occur in the propeller plane. The

third plane is the 'ESD plane' and indicates where the PSS will be located. This plane is located 1.65m upstream for the propeller plane.
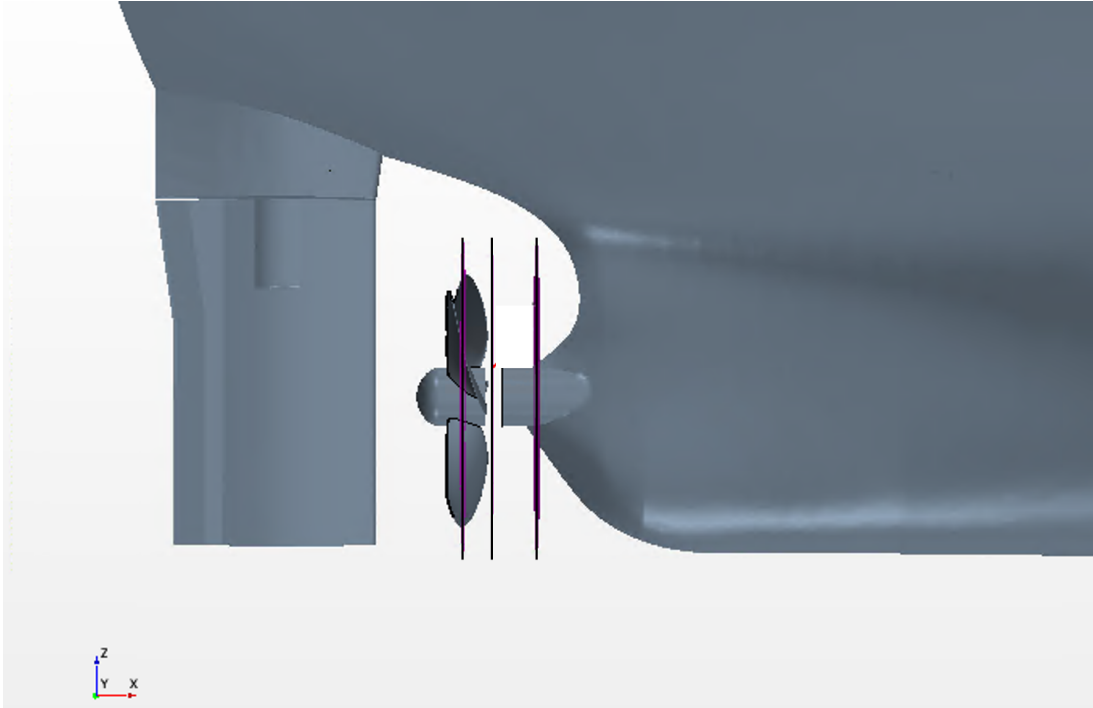
Figure 4.5: Relevant plane sections in the simulations

Chapter 5

Results

This chapter presents the simulation results obtained from Star-CCM+. First, the simulations with free surface are discussed. These provide the ship's resistance coefficient including the wave making resistance. Then the results from the simulations using double-body model are presented, including the resistance coefficient without free surface, nominal and effective wake of the ship. Following the results from the optimization will be presented. Through an optimization study, multiple design configurations will be investigated in order to find the optimal design configuration.

5.1 Numerical investigation

To validate the set-up for the simulations, multiple analyses were performed to check if the set-up was adequate. There are many elements that influence the results of the simulations, and to evaluate whether the set-up was satisfactory, the results were compared to the work done by Koushan et al. (Koushan et al., 2020).

5.1.1 Domain with free surface

Ship resistance

To obtain similar results as Koushan et al. did in their study with the same ship, multiple meshes and physics conditions were investigated. To validate the mesh in the simulations, the ship resistance coefficient, C_{TS}, was compared to Koushan et al. (2020)'s results. This coefficient include contributions from pressure, friction and wave making resistance.

The main difference between the three meshes is how the cells are distributed throughout the domain. Mesh 1 has finer mesh in the domain, but the mesh refinement close to the hull was not created correctly. The prism layer mesh failed to solve properly for the velocities in the boundary layer, and this strongly influenced the results. Mesh 2 has a better refinement in the boundary layer, but still resulted in quite high Y+ values because the prism cells in the boundary layer were too coarse. Mesh 3 had satisfactory refinement close to the ship, but was coarser in the main domain. This was implemented to keep the cell count low while it did not influence the results much. Mesh 3 gave considerably closer results to Koushan et al.. Table 5.1 sums up the results for the total resistance coefficients for the different mesh refinements. Mesh 3 gives satisfactory results and is used as base of the remainder of the simulations.

Table 5.1: Total resistance coefficient for different mesh refinements

| Mesh configuration	C_{TS}	ΔC_{TS}	Number of cells
Mesh 1	0.00250	8.7%	7300000
Mesh 2	0.00215	-6.5%	9300000
Mesh 3	0.00233	1.3%	10730000

Wave making

Figure 5.1 displays the developed wave pattern from the simulation with free surface. In the figure, one can see the general Kelvin wake pattern with a lateral and a transverse wake which is expected for a ship in motion. A detailed analysis of the wave pattern has not been performed in this project, but this plot of the wave elevation shows that the solution makes physically sense. This also imply that the time step used for the free surface simulation is sufficiently small.
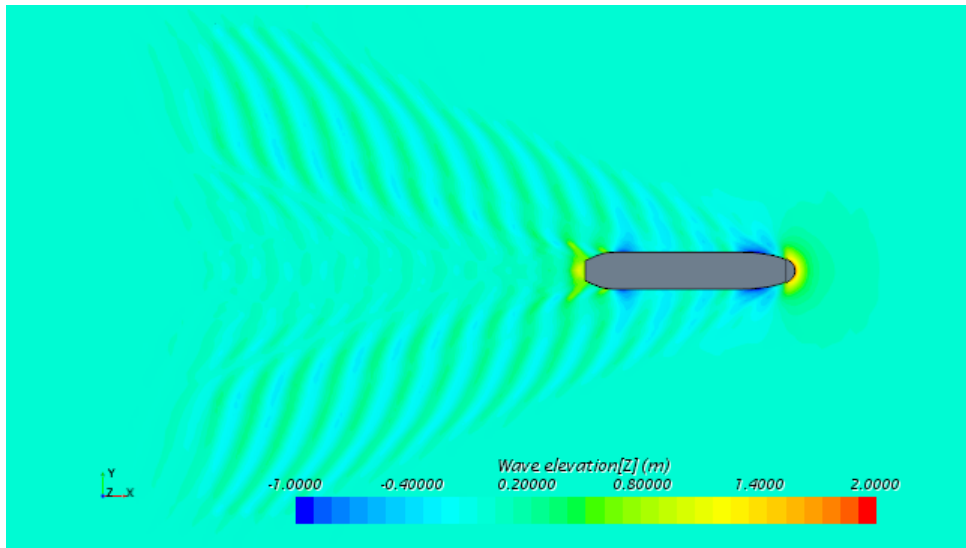
Figure 5.1: Wave pattern in free surface

Figure 5.2 shows the wave elevation at the hull using rhw volume of fluid model. This figure visualize how air and water is distributed in the domain.
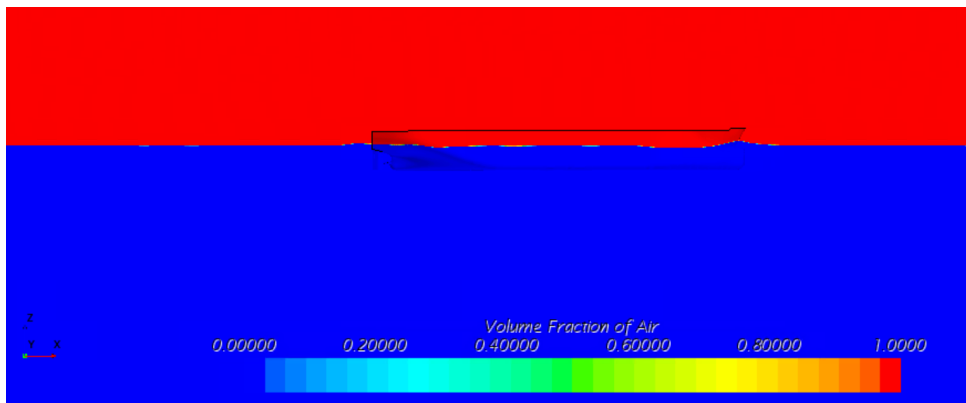
Figure 5.2: Wave elevation

5.1.2 Domain without free surface

To achieve faster convergence, and thus shorter computational time, the free surface is replaced by a double-body model. Instead of a free surface, there will be a symmetry plane at the waterline. This domain saves computational effort because the VOF-equation does not have to be solved, and there are fewer cells in the domain.

Resistance

The next step in the verification process of the numerical set-up is to investigate the resistance coefficient, C_{TS}, without free surface. The resistance coefficient is calculated using a rotating propeller, and the results are compared to the study of Koushan et al.. The resistance coefficient to be investigated include the contributions from additional resistance that originate from wave-making resistance, bilge keels, tunnel thrusters, and aerodynamic resistance. The wave-making resistance is assumed to be the difference between the free surface resistance and the resistance without free surface and without implemented propeller. The ship resistance coefficients for the different simulation configurations are listed in Table 5.2.

**Table 5.2:** Ship resistance coefficients for different simulation configurations

Resistance	C_{TS}
With free surface	0.00233
Without free surface, without propeller	0.00205
Without free surface, with rotating propeller	0.00271
Included additional resistance	0.00308

The ship resistance coefficient with all additional factors is calculated to be 0.00308. Koushan et al. presents a value of 0.002976 for the ship resistance coefficient in their paper, giving a 3.5% difference between the current set-up and the set-up used in their simulations (Koushan et al., 2020). These results are considered as satisfactory for this study and the optimization process of the pre-swirl stators.
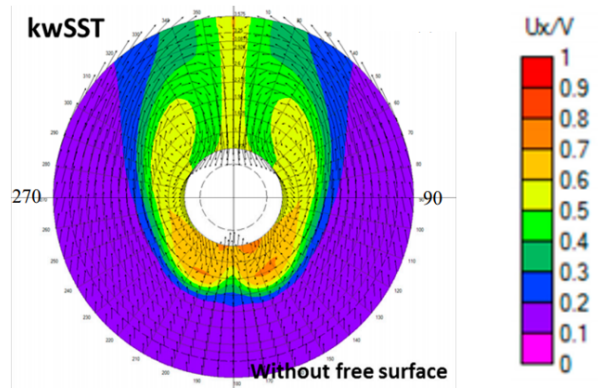
5.1.3 Nominal wake

The full-scale nominal wake field is obtained from the CFD simulations. These simulations are performed with the naked hull, meaning that the propeller and pre-swirl stator are disregarded. The nominal wake field for this set-up is compared to the wake field from the simulations performed by Koushan et al. as a part of the verification process for the simulation set-up.

Figure 5.3a show the full-scale nominal wake computed in Star-CCM+ from the naked-hull simulations, and Figure 5.3b is the full-scale nominal wake field obtained by Koushan et al.. The nominal wake fields show good agreement for the comparison of axial and transverse velocities. The isolines present the axial velocities, and the vectors present the transverse velocities. It is possible to see that the isolines of the axial velocities seem to be changing similarly at the same places, and the velocities have roughly the same values. From both figures, one can see that the vortices on port side and starboard side give a rotation clockwise and counter clockwise, respectively. These vortices originate from the motion of the flow around the hull.
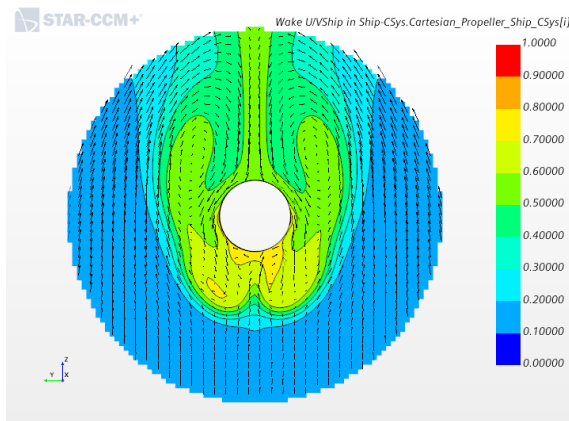
(a) Nominal wake with Star-CCM+

(b) Nominal wake presented in Koushan et al.s study (Koushan et al., 2020)

Figure 5.3: Nominal wake at the propeller plane

5.1.4 Effective wake field

The effective wake field is an important tool to get a visual presentation of the velocities coming into the propeller. The effective wave field can be used when predicting the hydrodynamic performance of the propeller. Figure 5.4 illustrate the effective wake field at section 'Inflow' 0.6 meter in front of the propeller. The transverse velocities are also plotted with a scale in Appendix A.1.
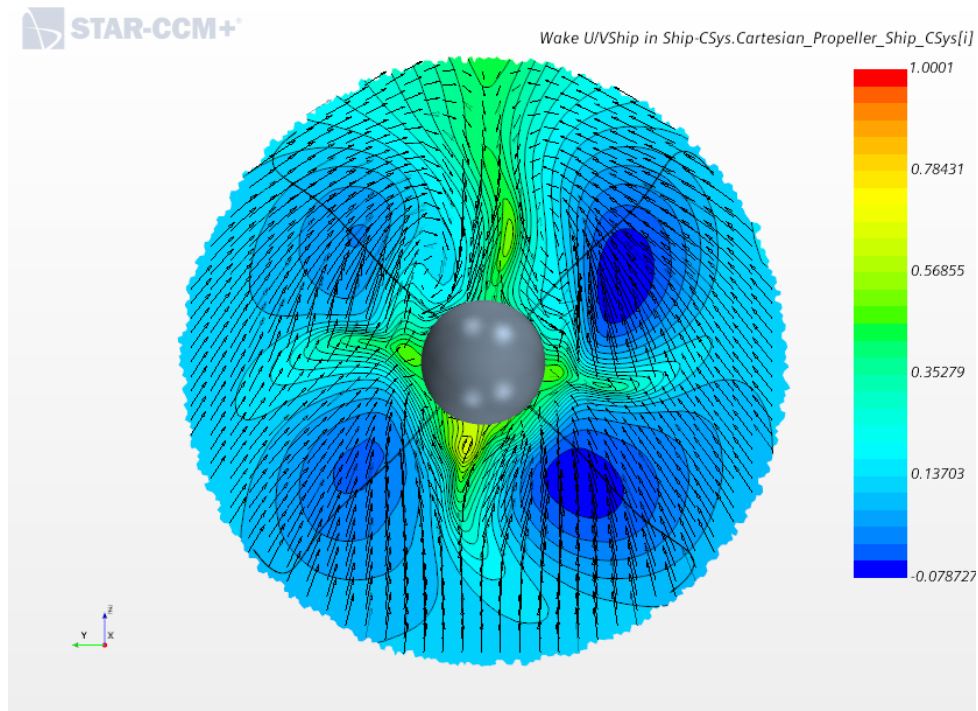
Figure 5.4: Effective wake field

5.2 Fin radius

To find the optimal fin radius for the pre-swirl stator, multiple simulations was run using various fin radii and the results are compared to the corresponding simulations without fins. The radii used in the simulations are 0.9R, 1.0R, 1.05R, 1.077R and 1.10R. To decide which radius provides the most desirable results, the thrust, T, delivered power, PD, and resistance are compared. It is also interesting to compare the transverse and axial velocity in front of the propeller.

When the flow is influenced by the pre-swirl stator, the propeller will deliver an increased level of thrust. Figure 5.5 show how the delivered thrust is increased for all fin radius configurations. In general, fins with radius 1.1R, 1.077R and 1.05R increase the delivered thrust the most.

It is necessary to study how the delivered power is influenced by the different fin configurations. The delivered power is proportional to the torque on the propeller as seen in Equation 2.5, thus it is desirable to keep the torque as low as possible to reduce the fuel consumption. Figure 5.6 shows how much the delivered power is increased for the different fins. Similar to what is observed for the thrust, the longer fins seems to increase the delivered power the most.
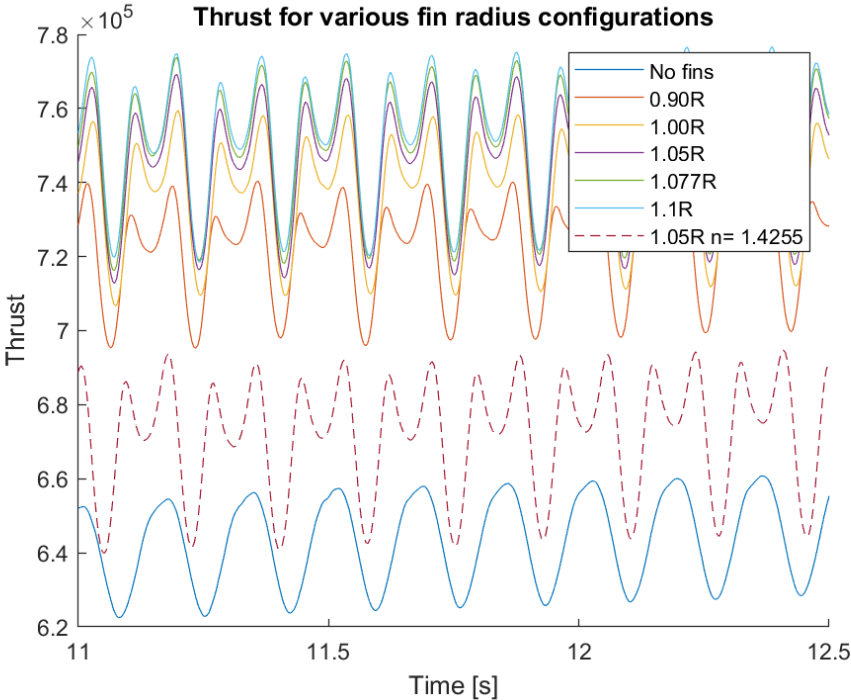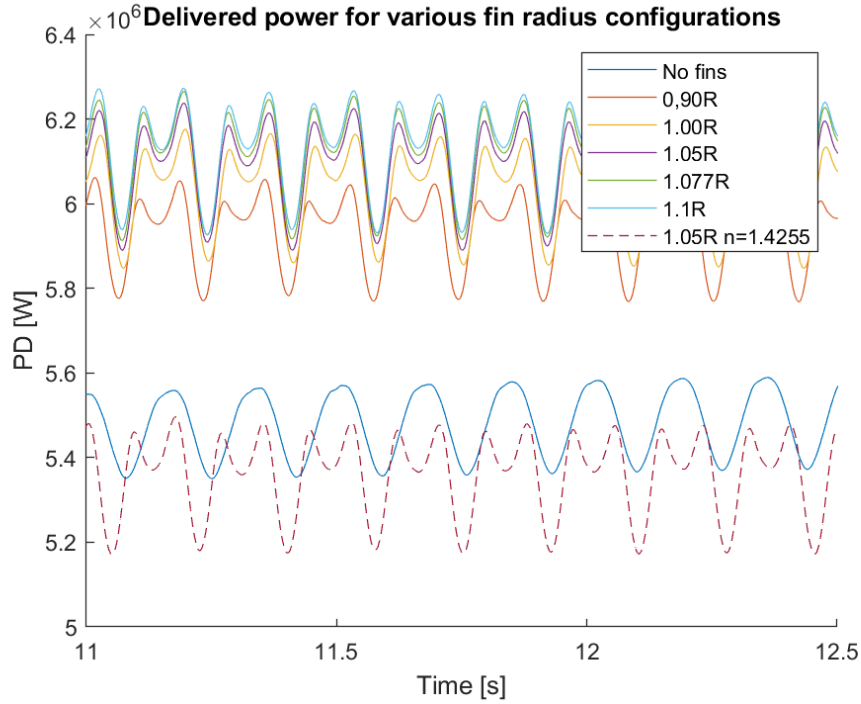

Figure 5.5: Thrust $T[N]$ for various fin radii

**Figure 5.6:** Delivered power, $PD[W]$, for various fin radii

In the process of finding the most optimal fin radius it is desired to find the configuration that offers the largest increase in thrust while keeping the delivered power as low as possible. Therefore it is valuable to evaluate the increase in propeller efficiency, which indicate the relation between how much the thrust has increased compared to the increased delivered power with the implemented PSS. Table 5.3 shows the average increase propeller efficiency and the average increase of resistance. The average values are calculated over one period for all fin radii. It is evident that the largest fin radius provides the greatest increase of propeller efficiency. This configuration does also have the largest increase in ship resistance.

Table 5.3: Increase in propeller efficiency and ship resistance for various fin radii

Fin radius	$\Delta\eta_P$	ΔR_{TS}
Without fins	1.0000	1.000
0.90R	1.0377	1.033
1.00R	1.0436	1.041
1.05R	1.0456	1.044
1.077R	1.0466	1.047
1.10R	1.0469	1.186
1.05R n=1.4255	1.0682	1.031

Figure 5.7 show the resistance plot for the ship when different pre-swirl stators are implemented. When pre-swirl stators are added to the ship, the resistance increase due to added wetted surface and altered flow pattern. From the resistance plots is is possible to see that the longest fins give the highest value of resistance for the ship. Although the resistance for the longest fin radius gave suspiciously high values, it can be noted a trend of increased resistance for the longer fins.

This must be taken into account when evaluating the optimal pre-swirl stator configuration. The increase in resistance must not outweigh the increase in propeller efficiency.
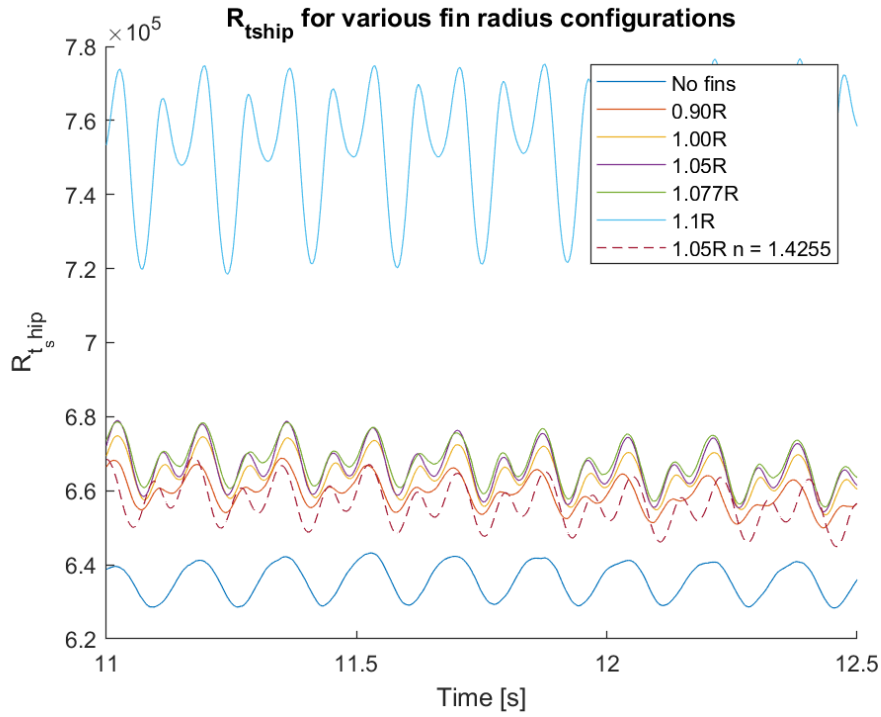
Figure 5.7: Resistance, $R_{tship}[N]$ for different radius of the stator fins

Increased thrust and constant rotational speed on the propeller will lead to increased resistance for the ship. Therefore it is desired to investigate how the resistance change when the propeller rotational speed is decreased. From the propeller efficiency results in Table 5.3 and the resistance plot in Figure 5.7 the fin with radius 1.05R is found to provide the best results when also considering the increase in resistance. To get closer to the propulsion point and increase the propeller efficiency, this configuration was simulated one more time with a lower propeller rotation speed. The rotation speed is decreased with 3% from 1.4720 to 1.4255 rps, and in Figure 5.5, Figure 5.6 and Figure 5.7 the plots are shown with dashed lines. With the lower rotation speed the thrust and delivered power are considerably reduced, but the propeller efficiency is considerably increased, as shown in Table 5.3. From Figure 5.7 one can see that this results in the lowest increase in resistance as well. The configuration with radius 1.05R and rotation speed 1.4255 rps will be used for the remainder of the simulations.

Figure 5.8 show how the transverse and axial velocities are influenced by the pre-swirl stators. Figure 5.8 is the effective wake field at section 'Inflow' in front of the propeller. Due to the PSS, there is an increase of flow retardation, meaning that the axial in front of the propeller velocities are decreased. In Appendix A.2 the transverse and axial velocities for all fin radii are presented.

(a) Without PSS   **(b)** Fin radius = 1.05R
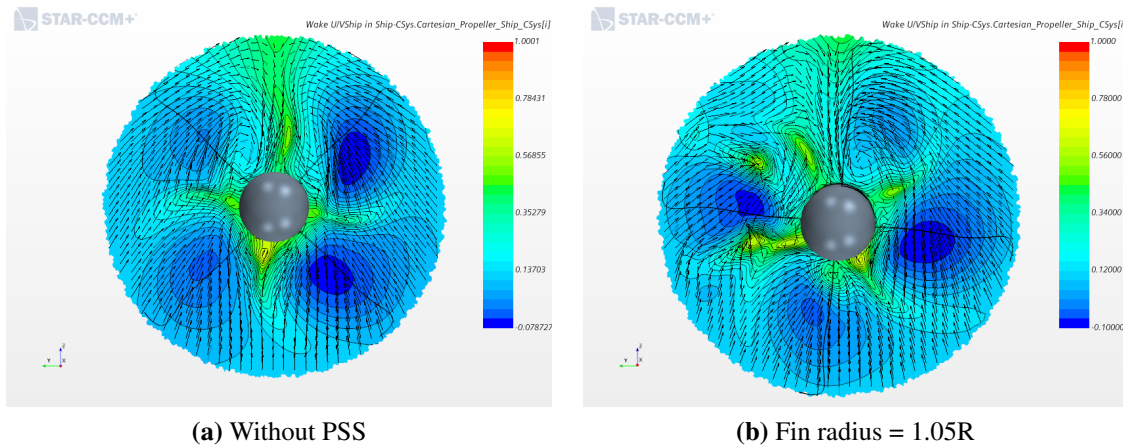
Figure 5.8: Distribution of the transverse and axial velocity on 'Inflow' section in front of the propeller without PSS and with fin-radius 1.05R

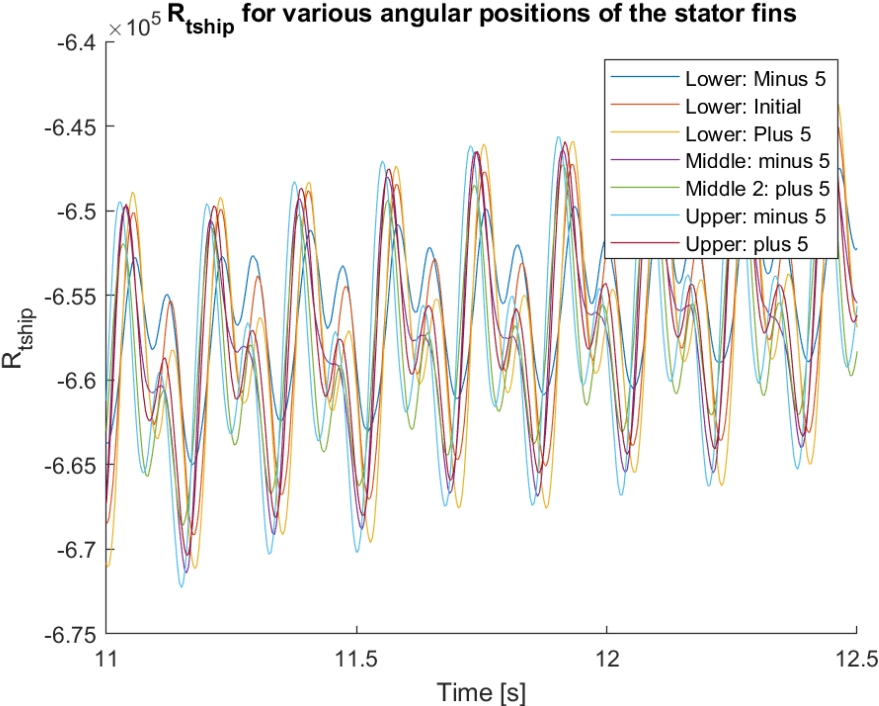# 5.3 Angular position of stator fins

The optimal angular position is found by adjusting the position of the stator fins and study the influence on the propeller efficiency and the resistance. Each of the fins are rotated five degrees clockwise and counter clockwise starting with the lower fin, then middle and at last the upper fin. Table 5.4 lists how the propeller efficiency vary with the different fin configurations. The optimal solution for each of the fins are marked with a check-mark indicating which angular position that provides the best results. From the results one can see that the best configuration is when the lower fin is rotated five degrees clockwise, the middle fin kept in initial position, and the upper fin is rotated five degrees counter clockwise.

Table 5.4: Configurations of angular positions investigated in the optimization process

Configuration	Upper	Middle	Lower	Propeller efficiency	Preferred config.
Lower fin optimization	22	67	108	1.0686	✓
	22	67	113	1.0682	
	22	67	118	1.0674	
Middle fin optimization	22	62	108	1.0678	
	22	67	108	1.0686	✓
	22	72	108	1.0681	
Upper fin optimization	18	67	108	1.0677	
	22	67	108	1.0686	
	27	67	108	1.0694	✓

From Table 5.4 it can be seen that the propeller efficiency does not change much among the different configurations. It differs only 0.2% from the lowest propeller efficiency to the highest, indication taht the angular position does not influence the propeller efficiency significantly. The same yields for the ship resistance. As plotted in Figure 3.7, the resistance does not change much when the angular positions are altered. Because the propeller efficiency and ship resistance are nearly constant for all configurations, it is not obvious which configuration to choose.

However, for the remainder of the simulations, the configuration having upper, middle and lower fins located at 27, 67, and 108 degrees from the z-axis is used since these angular positions gave slightly higher increased propeller efficiency. Figure 5.10 shows the angular position of the stator fins before and after the optimization. The fins indicated with pink color are the initial angular configuration, whereas the fins in gray are the optimized configuration. As seen in the figure, the middle fin is kept at its initial position, the lower fin is rotated 5 degrees clockwise, and the upper fin is rotated 5 degrees counter clockwise.

Figure 5.9: Resistance, $R_{tship}[N]$, for different angular positions of stator fins
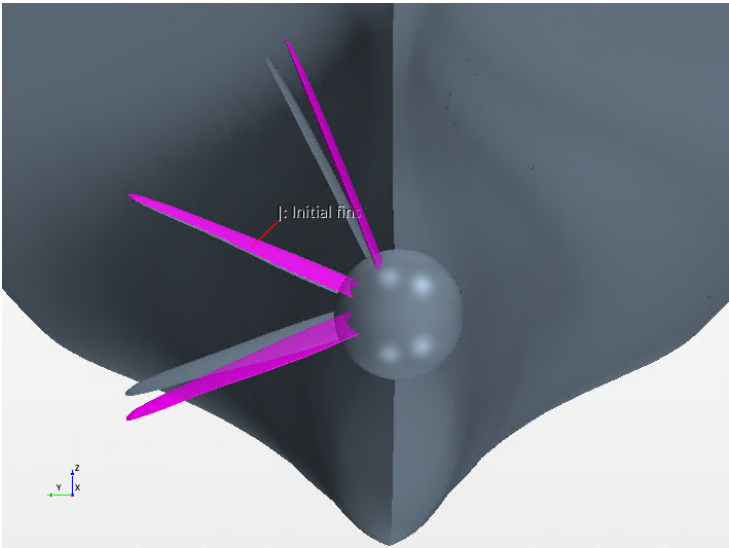
Figure 5.10: Initial angular configuration is indicated with pink color, and the optimized fins are indicated with gray

5.4 Stator pitch angle

The pitch angle of the stator fins are rotated in both directions from the initial configuration with increments of 4 degrees. Since this is the final step in the optimization process, the optimal configuration of the stator pitch angle will represent the final design.

From Table 5.5 it can be seen that the stator pitch angle strongly influence the propeller efficiency, $\Delta\eta_P$. The pitch of the stator fins is highly relevant when reorienting the flow into the propeller, and manipulation of the flow results in altered angle of attack for the propeller blades.

**Table 5.5:** Increase in propeller efficiency and ship resistance for various stator pitch angles

Stator pitch angle	$\Delta\eta_P$	ΔR_{TS}	Remark
83.0, 70.5, 61.0	1.0851	1.0472	Minus 8 degrees
87.0, 73.5, 64.0	1.0762	1.0399	Minus 4 degrees
91.0, 77.5, 68.0	1.0694	1.0331	Initial pitch position
95.0, 81.5, 72.0	1.0593	1.0253	Plus 4 degrees

Figure 5.11a-e provides a better insight on the influence of pre-swirl stators. These figures presents the tangential velocity distribution at the 'Inflow' plane in front of the propeller. These plots show how the various pre-swirl stators influence the flow around the propeller. Figure 5.11a shows the tangential velocity without pre-swirl stators, and Figure 5.11b, c, d, and e shows the tangential velocity for different pitch angles for the stator fins. These plots are also provided in Appendix A.3 for larger figures.

Positive tangential velocities are defined clockwise, and are represented in the red spectrum of the color bar. From Figures 5.11b, c, d and e, one can notice a reduction in positive swirl at the port side of the vessel. The pre-swirl stator breaks up the vortices from flow separation on the hull, and thus the tangential velocities on the port side is reduced. Since the propeller has a clockwise rotation, this means that the relative velocity between the flow and the propeller increase, and thus the angle of attack of change. The tangential velocities are also altered at starboard side of the vessel, although the PSS is located on port side. It is observed that all PSS configurations results in increased negative swirl in the outer sections of the propeller.

From Table 5.5 it was observed that the PSS configuration with fins pitch angle rotated minus 8 degrees results in the highest increase in propeller efficiency. This configuration also gives the highest added resistance, but since this study is performed with a fixed ship velocity and propeller rotational speed, the main focus is on the increase in propeller efficiency. This means that the best fin configuration is the one where the fins are rotated -8 degrees in pitch angle.
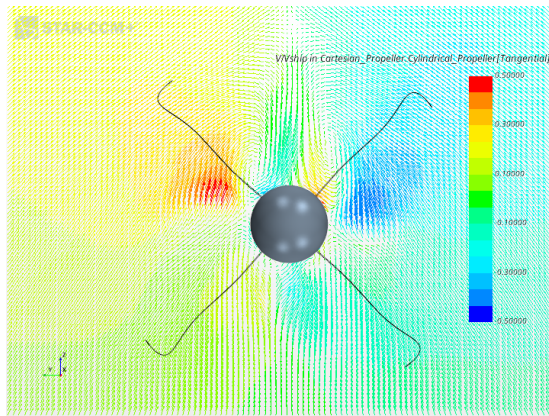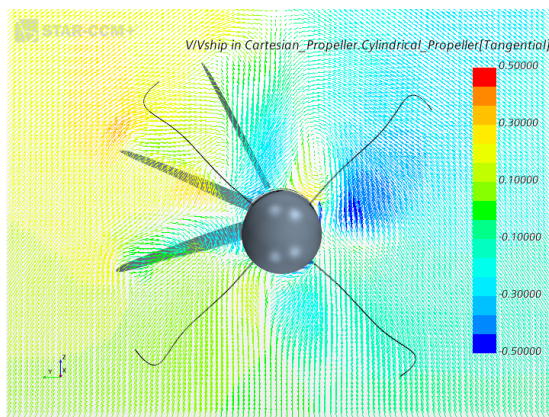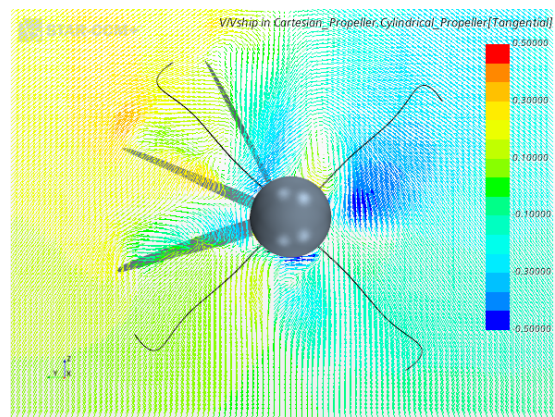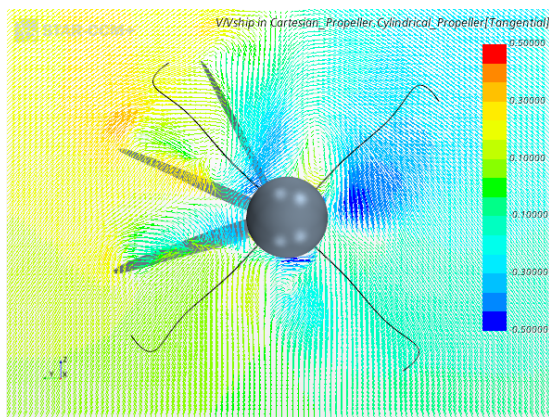
(a) Without fins
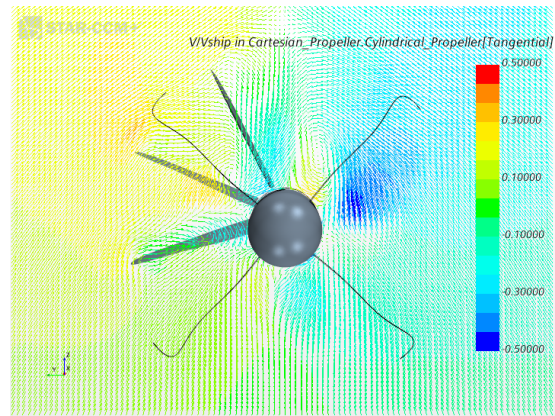
(b) Pitch rotated +4 degrees

(c) Pitch initial position

(d) Pitch rotated -4 degrees

(e) Pitch rotated -8 degrees

Figure 5.11: Distribution of the tangential velocity on 'Inflow' section in front of the propeller for various stator pitch angles

5.5 Optimized configuration

In this section a visualization of the influence of PSS is presented. For this study, the PSS design that resulted in the largest increase in propeller efficiency is used. From the optimization study, the optimal design parameters have been found to be a fin radius of 1.05R, angular position rotated to 27, 67, and 108 degrees from the z-axis, and pitch angle rotated -8 degrees from initial position. The propeller rotational speed has also been reduced with 3% from 1.4720 rps to 1.4255 rps, so move closer to the self-propulsion point.

From the following figures, the effect of the pre-swirl stator on the flow direction, pressure distribution and vorticity is investigated. Figure 5.12 and Figure 5.13 shows the streamlines at the hull, distribution of pressure coefficient at the hull and the hub vortex for the hull without PSS and with PSS, respectively. These figures illustrates how the pre-swirl stator serves a multipurpose through influencing the flow in different ways.

In Figure 5.12 the vortex due to separation in the stern area is detectable in the streamlines constrained to the hull. In Figure 5.13 one can see that the vortices in the stern area is canceled out by the pre-swirl stator. This provides a more uniform wake for the propeller so that the propeller blades are more heavily and uniformly loaded. This occurrence is what is happening in Figure 5.11b-e where the positive tangential velocities are reduced.

The streamlines from the hub is colored by the magnitude of the vorticity. The strength of the hub vortex is decrease when the pre-swirl stator is implemented. The hub vortex seems to be more concentrated right behind the propeller hub, and is more parallel to the x-axis. The kinetic energy in the flow behind the hub is reduced, from reduction of tangential velocity. Behind the propeller, the tangential component creates rotational kinetic energy losses in the swirl. These tangential components of kinetic energy does not give any acceleration of fluid that contribute to the propulsion of the ship, so is is desired to reduce them.

When investigating the pressure coefficient for the hull and rudder, it can be seen that the pressure peak at the leading edge of the rudder is reduced from the PSS. In this scale the differences in pressure coefficient is hard to investigate, so a better visualization of the pressure coefficient of the propeller blades is provided in Figure 5.14.
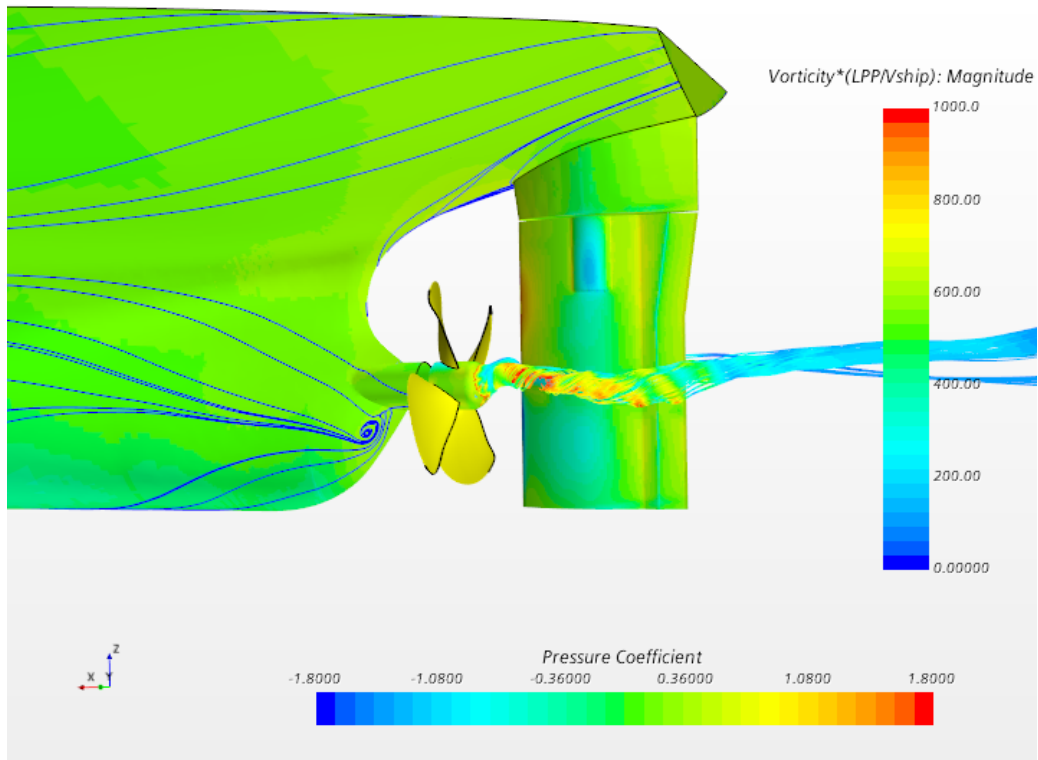
Figure 5.12: Streamlines over the stern and pressure coefficient distribution on the vessel surface withput pre-swirl stator
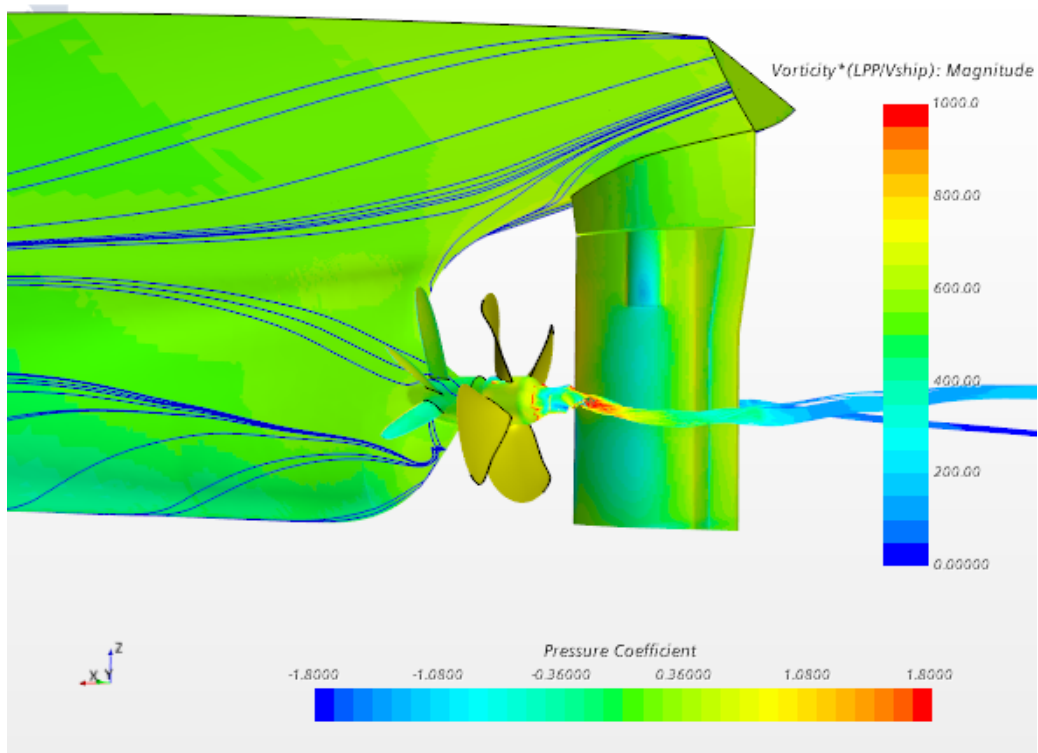

Figure 5.13: Streamlines over the stern and pressure coefficient distribution on the vessel surface with pre-swirl stator

Figure 5.14 shows the distribution of the pressure coefficient, C_P on the propeller hub and blades for the cases without PSS and the optimized PSS. The pressure coefficient imply the cavitation domains of the propeller, but is not a formal cavitation test, so a proper cavitation should also be performed.

At the hub the pressure difference is reduced due to weaker hub vortex. The propeller blades experience a favorable effect on the pressure coefficient on the suction side. With pre-swirl stator, the suction side experience a smaller area with the lowest pressure coefficient.

The low pressure coefficients on the suction side of the configuration should be investigated. Root cavitation could be a problem for propellers with implemented pre-swirl stators. For these locations, the local cavitation number, σ_0 should be evaluated to assess the risk of cavitation. On the pressure side of the propeller in Figure 5.14c the pressure coefficient is observed to increase at the blade tip in the wake peak area. This could indicate risk of tip cavitation, that could result in damages on the propeller, vibration, noise or other undesirable effects from cavitation.

(a) Pressure side without PSS

(b) Suction side without PSS

(c) Pressure side with PSS

(d) Suction side with PSS
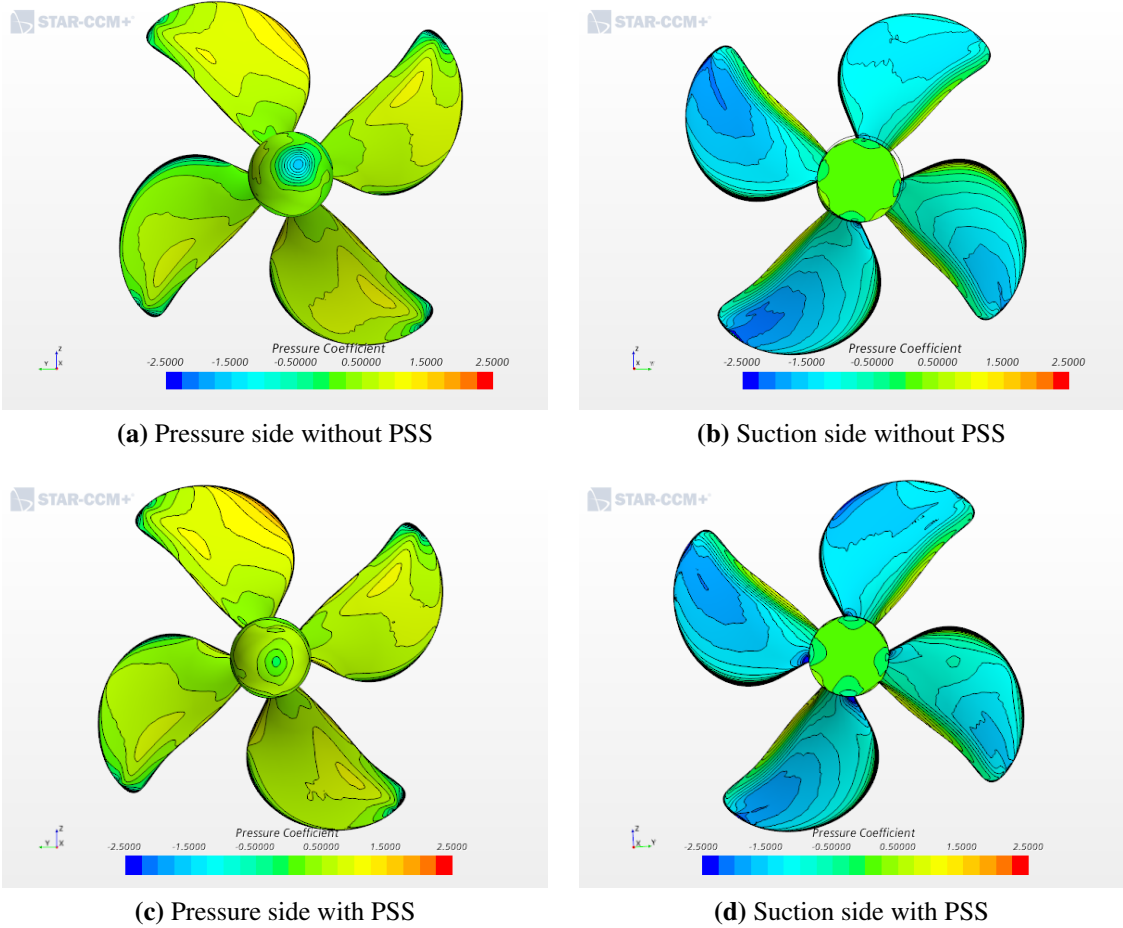
Figure 5.14: Pressure coefficient contours on the surface of the propeller blade

Chapter 6

Conclusion

A series of numerical simulations have been performed to optimize a pre-swirl stator for a chemical tanker. A comparison study verified the numerical set-up, and through several iterations of the mesh and physical set-up, the results was satisfactory. The verification process shows that the numerical results have good agreement with the study performed by Koushan et al.. The comparison study investigated the nominal wake and the resistance coefficient for the ship with and without free surface. The free surface simulations was used in the validation process of the numerical set-up. Double-body model was later implemented to save considerable computational time. The obtained values for the resistance coefficient was found to be almost identical to the aforementioned study and was found to be within acceptable range. The results from this study showed that the set-up was adequate for the optimization study of the pre-swirl stators.

16 different pre-swirl design configurations were investigated in the optimization process. By systematic variation of the design parameters, the various configurations were investigated through numerical computations. The optimal design parameters were found through investigation of the propeller efficiency, wake, and increase in resistance. The velocities into the propeller were studied to understand how the pre-swirl stators influence the flow into the propeller. The propeller experience a modified angle of attack when the inflow velocities are altered. This means that the rotational speed of the propeller can be reduced, while still experiencing the same effective angle of attack, and thus reduce the energy demand. The propeller rotation was reduced by 3%, and this showed significant results.

From the simulations, it shows that the stator fin radius and the stator fin pitch angle had the most significant influence on the propeller efficiency. It was evident that the angular position did not influence the propeller efficiency notably. Nine different angular positions of the fins were investigated, but none of the configurations stand out. This may imply that the angular position was not varied enough, or that it does not influence the flow to a large extent.

From the results, it is evident that all design configurations gave an increased propeller efficiency compared to the case without PSS. The objective of the thesis was to increase the propeller efficiency, so that the fuel consumption of the ship is reduced. The optimal design gave an increase in propeller efficiency by 8.51% compared to the case of no PSS, and 3.85% more than the initial PSS configuration. This is deemed satisfactory results, and would contribute to a reduced fuel consumption. This design configuration increase the average relative resistance with 4.72% compared to the ship without PSS. Since the study was carried out with a fixed rotational velocity of the propeller, the resistance increase when the thrust increased. Increased resistance does not weigh in as heavy as the increased propeller efficiency for the decision of which PSS configuration is optimal, since the resistance could go down with another propeller rotation velocity.

From analyzing the results from the simulations, it is found that the hub vortex is reduced by the PSS, and the swirl in front of the propeller is canceled out. The pressure distribution is also influenced when the PSS is implemented. On the propeller the low-pressure area decrease, but new low-pressure areas appear near the root of the propeller. This should be further investigated.

6.1   Further work

6.1.1   Propeller boss cap fins

A possible extension to the work in this thesis would be to investigate the potential of implementing propeller boss cap fins, PBCF, in combination with the pre-swirl stator. These are compatible devices, and the PBCF could make use of the remaining energy in the hub vortex and thus provide additional energy reduction for the ship. In Figure 5.13 it is evident that despite implementation of a PSS, there will still excist a hub vortex behind the propeller. A implementation of PRBC to reduce the hub vortex, could also result in reduced stern vibration, provide lower propeller noise and reduce risk of rudder erosion.

The PBCF may also be designed to provide additional lift from the kinetic energy. Using the numerical set-up presented in this thesis, a potential next step would be to assess whether additional reduction of energy losses is possible be by implementing a PBCF. The PSS and the PBCF would also influence the rudder, since there will be less rotational energy to utilize. Thus, it is crucial to include the interaction phenomena for the entire system including hull, ESD's, rotating propeller and rudder.

6.1.2   Other optimization parameters

In this project the stator was optimized for the design parameters fin radius, angular position and fin pitch angle. Other fin geometry parameters such as fin tip radius, distribution of chord length and thickness of fin could also be targets for further investigation. Also installation parameters such as longitudinal position of PSS plane and number of fins could have been investigated further to see if it is possible to improve the propeller efficiency even more than what is found in this study.

In the simulations the propeller rotational speed is fixed. Since the simulations are not set up as self-propulsion tests the velocity does not increase even if the thrust of the propeller is increased. Preferably, the simulations should have been performed through a self-propulsion simulation. An alternative study would be to investigate how variation of rotational speed influence the results.

The propeller performance should also be verified at other speeds and drafts since these parameters will influence the inflow to the ESD and propeller. All simulations performed in this thesis is performed at design point of the ship with a velocity corresponding to 14 knots and draft of 11.846m.

6.1.3 Optimization method

Through a formal optimization study, for example generic algorithm or particle swarm optimization, the coupled effect between each of the parameters could have been studied. This method would have tested more combinations of the design parameters together, and better configurations could have been detected. A optimization study like this would require extensive computational power since there would have been more possible combinations to investigate.

For a formal optimization study, it would be beneficial to design the workflow of the optimization so that the design exploration is partially automated. One example of a partial automation of the optimization process is use of makros in the numerical simulations. That would save considerable amount of time, since the input to the simulations would have been updated automatically.

6.1.4 Propeller cavitation analysis

From the results it is seen that the pre-swirl stator that provides the highest increase in propeller efficiency have some areas where the pressure coefficient should be investigated further. Through a formal cavitation test, it could be clarified how big the risk of cavitation is in this environment. PSS have a tendency to increase risk of root cavitation on the propeller, thus a cavitation analysis would be of high value.

Bibliography

ABS, 2013. Ship Energy Efficiency Measures Advisory. ABS Report.

Baek, D.G., Yoon, H.S., Jung, J.H., Kim, K.S., Paik, B.G., 2015. Effects of the advance ratio on the evolution of a propeller wake. Computers and Fluids 118.

Bertram, V., 2011. Practical Ship Hydrodynamics. Second Edition, Elsevier.

Carlton, J., 2007. Marine propellers and propulsion. Butterworth-Heinemann.

CD-Adapco, 2016. Star-CCM+ User Guide v11.06.

Cengel, Y., Cimbala, J., 2010. Fluid Mechanics Fundamentals and Applications. Second edition in SI units, McGraw-Hill Higher Education.

Dang, J., Guoxiang, D., Chen, H., 2012. An exploratory study on the working principles of energy saving devices (esds) - piv, cfd investigation and esd guidelines. Proceedings of the 31st International Conference on Ocean, Offshore and Arctic Engineering OMAE2012 July 01-06, 2012, Rio de Janeiro, Braz .

Johansen, S., 2019. Literature study on energy saving devices. Project thesis .

Kawamura, T., Ouchi, K., Nojiri, T., 2012. Model and full scale cfd analysis of propeller boss cap fins (pbcf). Journal of Marine Science and Technology 17, 469–480.

Kerwin, J.E., 2001. Hydrofoils and propellers, lecture notes.

Kim, K., Leer-Andersen, M., Werner, S., Orych, M., Choi, Y., 2013. Hydrodynamic optimization of pre-swirl stator by cfd and model testing. Papers from the 29th Symposium on Naval Hydrodynamics .

Koushan, K., 2018. Foil and propeller theory (2018) - compendium. Lecture notes in TMR4220 Naval Hydrodynamics at NTNU.

Koushan, K., Krasilnikov, V., Nataletti, M., Sileo, L., Spence, S., 2020. Experimental and numerical study of pre-swirl stators pss. Journal of Marine science and Engineering .

Liseikin, V.D., 2010. Grid Generation Methods. Scientific Computation, Springer Netherlands, Dordrecht.

Nojiri, T., Ishii, N., Kai, H., 2011. Energy saving technology of propeller boss cap fins (pbcf) and its evolution. Journal of the JIMEVol. 46 No. .

Nowruzi, H., Najafi, A., 2019. An experimental and cfd study on the effects of different pre-swirl ducts on propulsion performance of series 60 ship. Ocean Engineering 173.

Park, S., Oh, G., Hyung Rhee, S., Koo, B.Y., Lee, H., 2015. Full scale wake prediction of an energy saving device by using computational fluid dynamics. Ocean Engineering .

Peric, M., Bertam, V., 2011. Trends in industry applications of computational fluid dynamics for maritime flows. Journal of Ship Production and Design, Vol. 27 .

Pettersen, B., 2019. Lecture notes in the course Numerical Methods in Marine Hydrodynamics.

Przybylski, M., 2015. Code saturne installation, validation and application .

Regener, P., Mirsadraaee, Y., Andersen, P., 2018. Nominal vs effective wake fields and their influence on propeller cavitation performance. Journal of Marine Science and Engineering; Basel Vol. 6, Iss. 2, .

Savio, L., 2011. Lecture note on Propeller cavitation. For lectures in TMR4220 Naval Hydrodynamics.

Sun, Y., Su, Y., Wang, X., Hu, H., 2016. Experimental and numerical analyses of the hydrodynamic performance of propeller boss cap fins in a propeller-rudder system. Engineering Applications of Computational Fluid Mechanics 10, 145–159.

van Terwisga, T., 2013. On the working principles of energy saving devices. Third International Symposium on Marine Propulsors smp'13 .

c. Wilcox, D., 2006. Turbulence Modelling for CFD. Third edition, DCW Industries.

Wärtsilä, 2017a. Wärtsilä energoflow boosts propulsion efficiency. URL: https://www.wartsila.com/twentyfour7/in-detail/wartsila-energoflow-boosts-propulsion-efficiency.

Wärtsilä, 2017b. Wärtsilä energoflow: For improved energy efficiency. Product brochure .

Appendix A

Results from CFD simulations
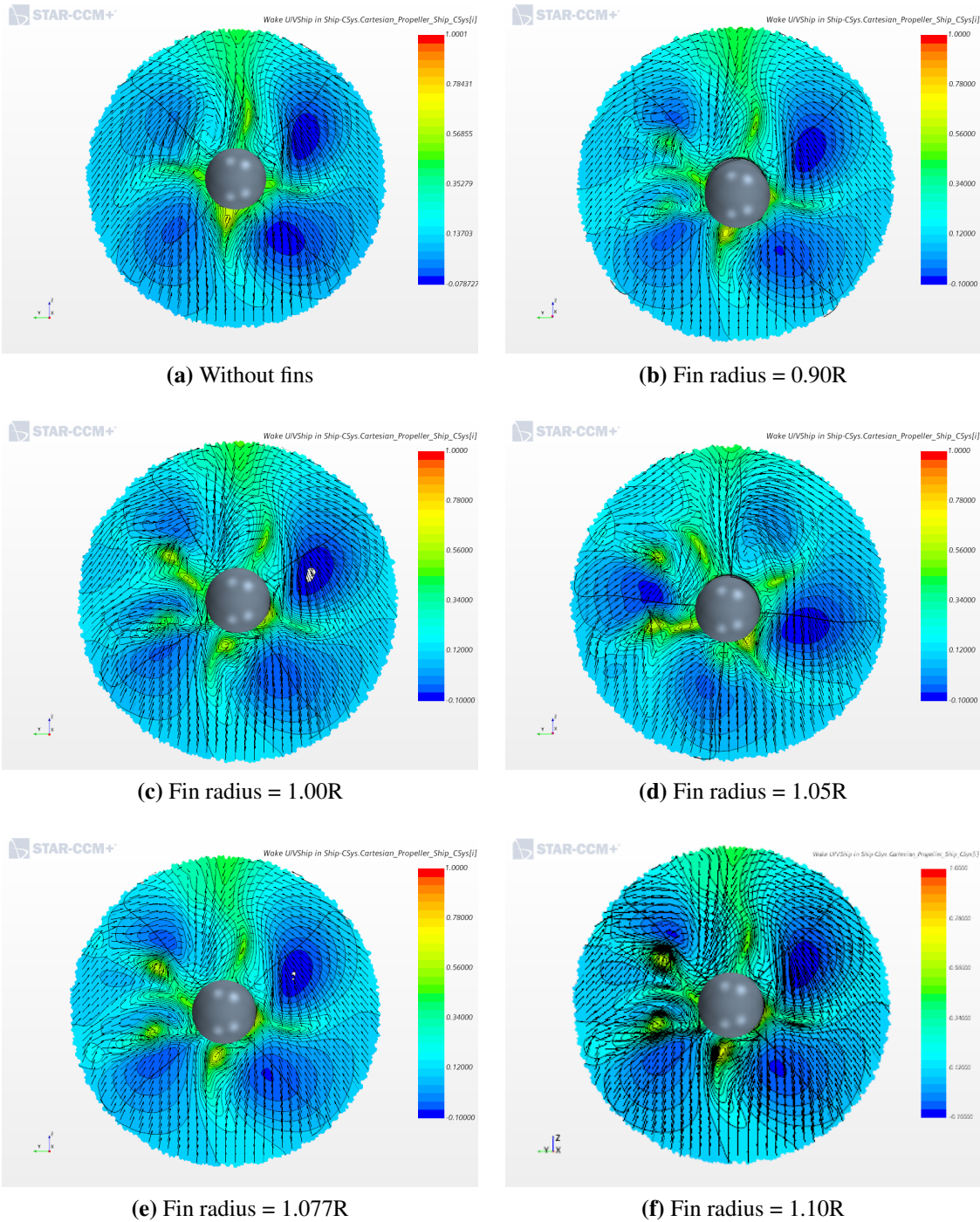
A.1 Effective wakefield
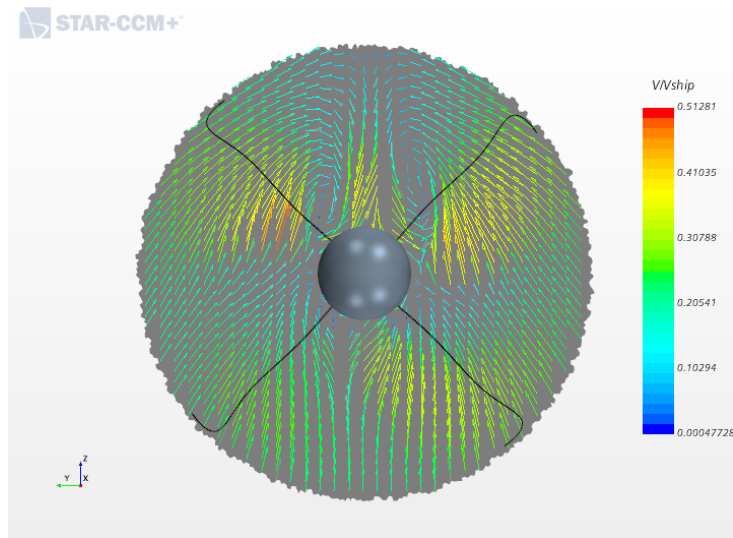
Figure A.1: Transverse velocities in effective wake field at section 'Inflow' in front of the propeller
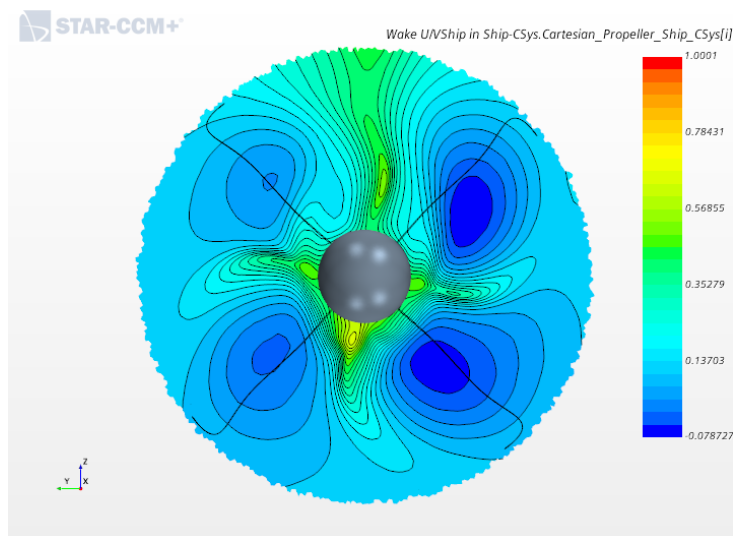
Figure A.2: Axial velocities in effective wake field at section 'Inflow' in front of the propeller

A.2 Fin radius optimization

(a) Without fins

(b) Fin radius = 0.90R

(c) Fin radius = 1.00R

(d) Fin radius = 1.05R

(e) Fin radius = 1.077R

(f) Fin radius = 1.10R

Figure A.3: Distribution of the transverse and axial velocity on 'Inflow' section in front of the propeller for various fin radii, seen from downstream

A.3   Pitch angle optimization
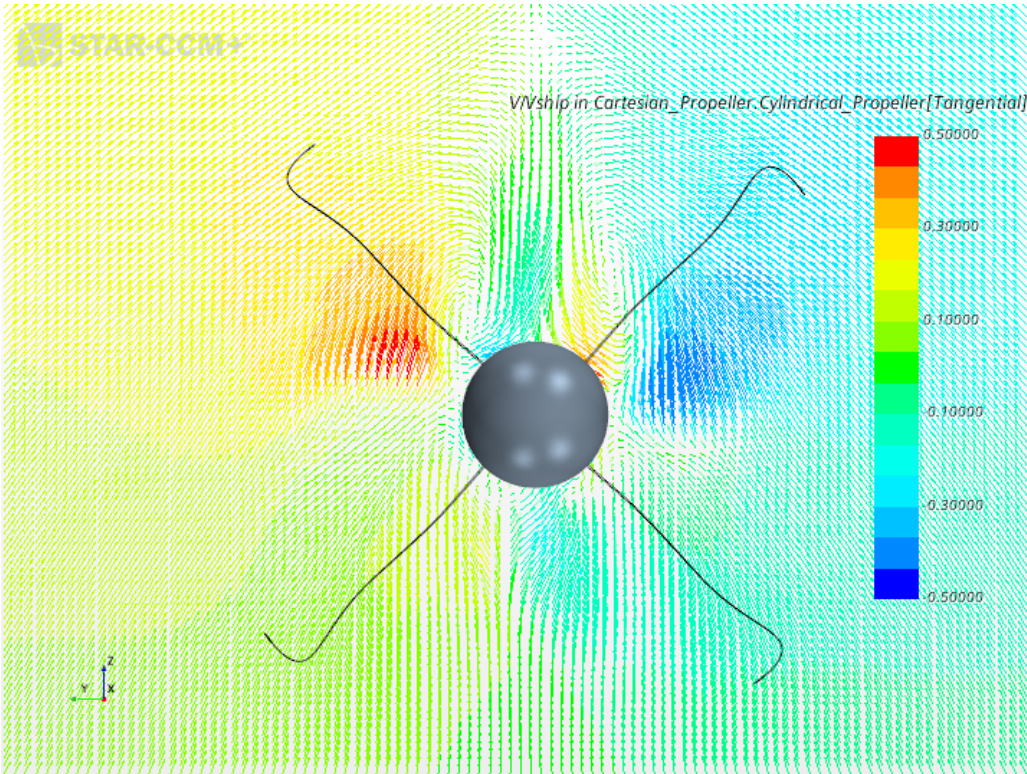
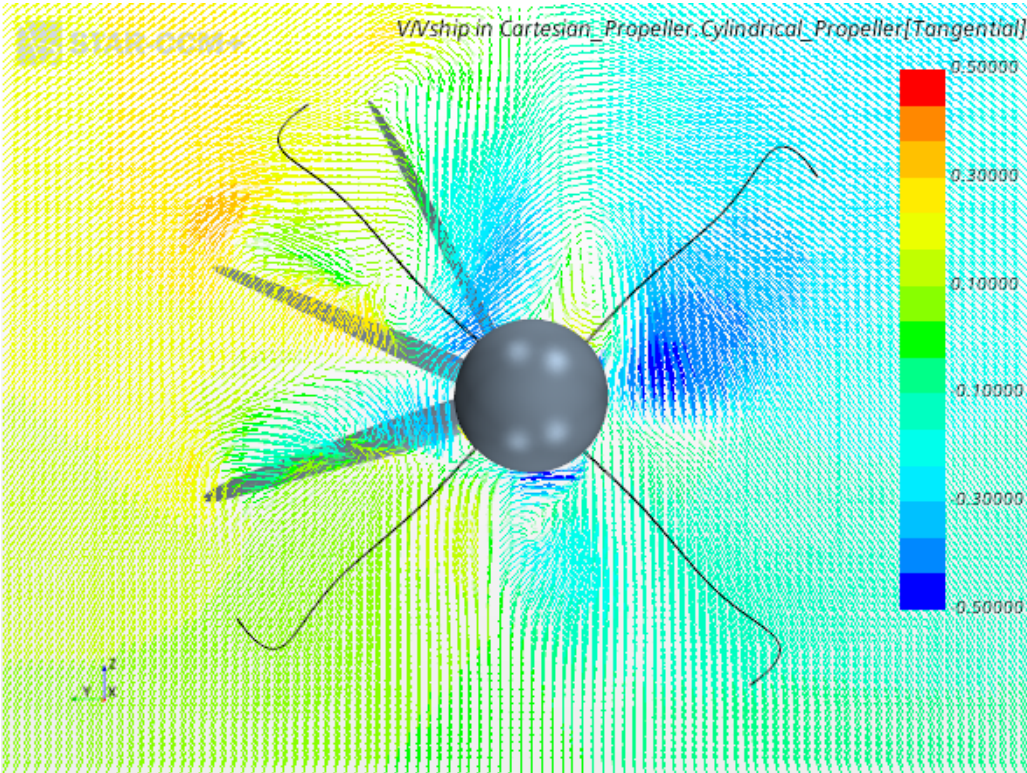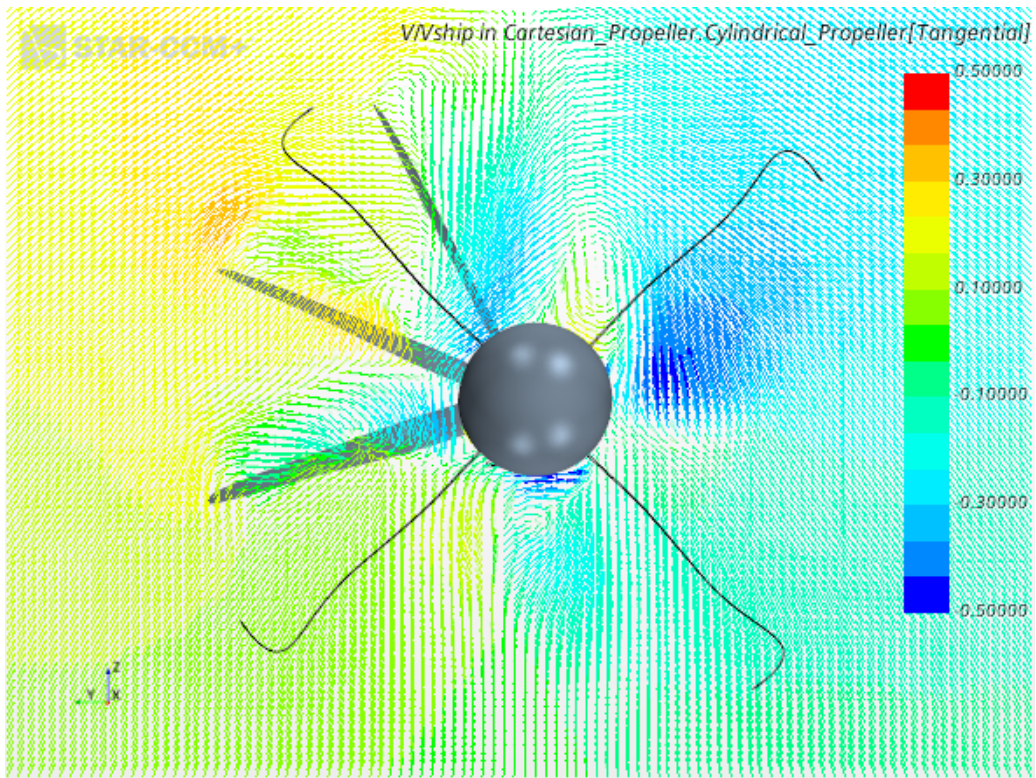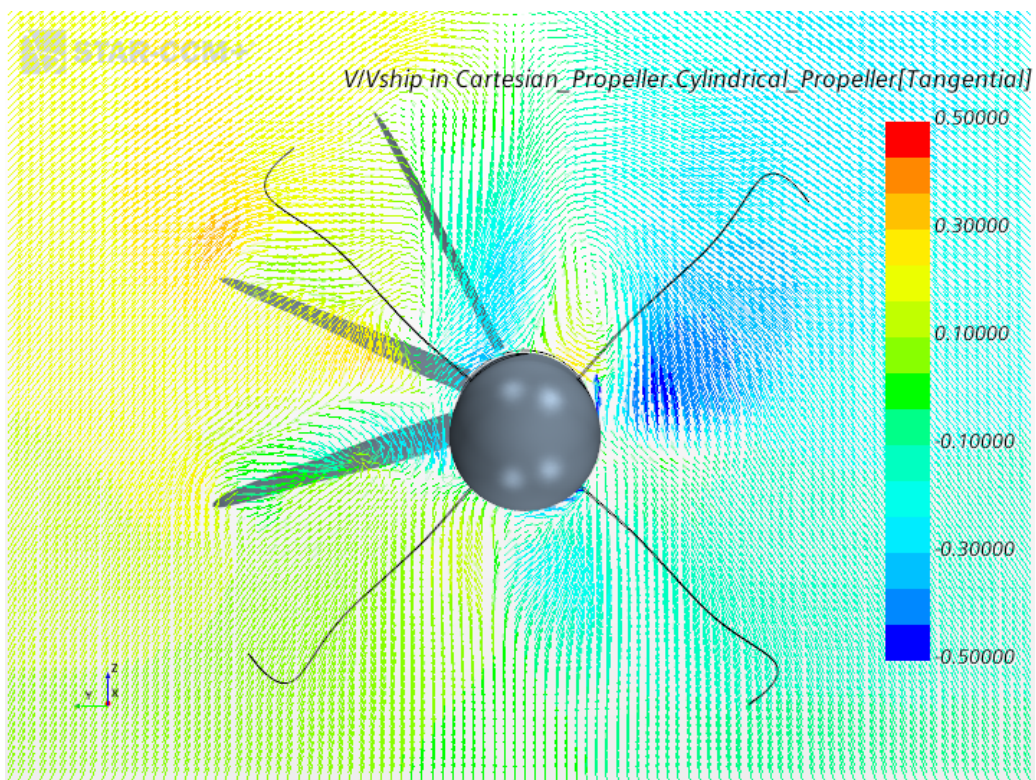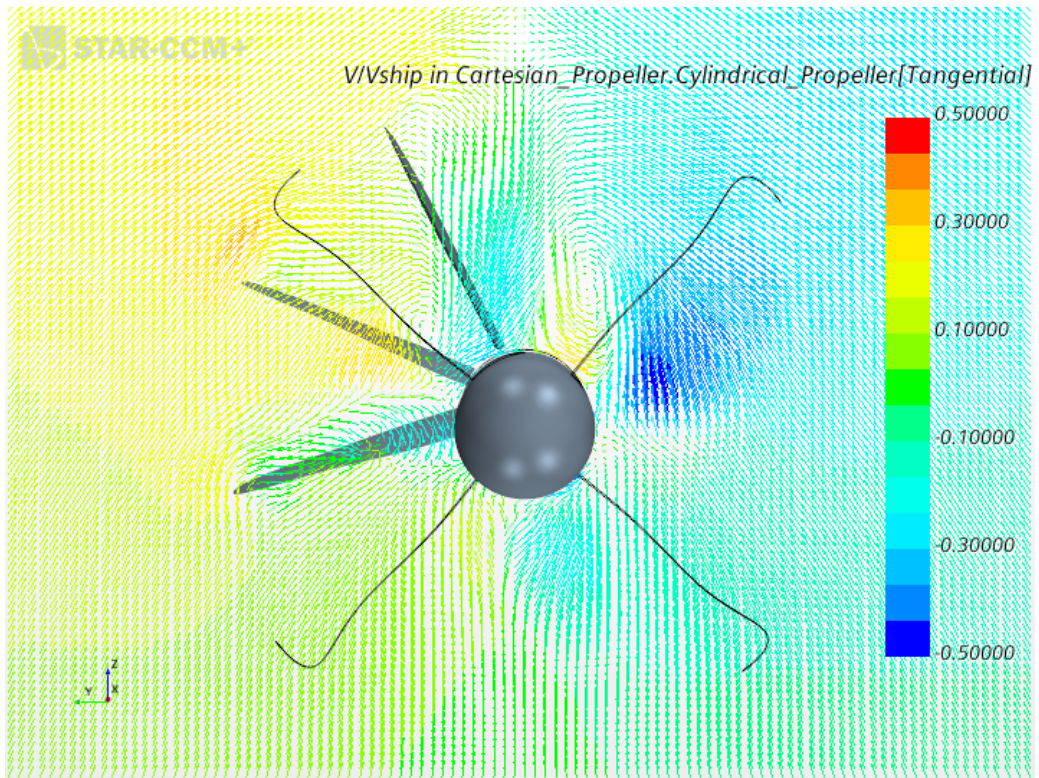**Figure A.4:** Tangential velocities at section 'Inflow' without PSS

Figure A.5: Tangential velocities at section 'Inflow' fins pitch rotated -8 degrees

Figure A.6: Tangential velocities at section 'Inflow' fins pitch rotated -4 degrees

Figure A.7: Tangential velocities at section 'Inflow' with initial pitch angle of the fins

Figure A.8: Tangential velocities at section 'Inflow' with initial pitch angle rotated +4 degrees